Critical examination of cohesive-zone models in the theory of dynamic fracture

J. S. Langer† and Alexander E. Lobkovsky‡
† *Physics Department, University of California, Santa Barbara, CA 93106*
‡ *Institute for Theoretical Physics, University of California, Santa Barbara, CA 93106*
(February 1, 2008)

We have examined a class of cohesive-zone models of dynamic mode-I fracture, looking both at steady-state crack propagation and its stability against out-of-plane perturbations. Our work is an extension of that of Ching, Langer, and Nakanishi (CLN), who studied a non-dissipative version of this model and reported strong instability at all non-zero crack speeds. We have reformulated the CLN theory and have discovered, surprisingly, that their model is mathematically ill-posed. In an attempt to correct this difficulty and to construct models that might exhibit realistic behavior, we have extended the CLN analysis to include dissipative mechanisms within the cohesive zone. We have succeeded to some extent in finding mathematically well posed systems; and we even have found a class of models for which a transition from stability to instability may occur at a nonzero crack speed via a Hopf bifurcation at a finite wavelength of the applied perturbation. However, our general conclusion is that these cohesive-zone models are inherently unsatisfactory for use in dynamical studies. They are extremely difficult mathematically, and they seem to be highly sensitive to details that ought to be physically unimportant.

I. INTRODUCTION

In a recent publication, Ching, Langer and Nakanishi [1] (CLN) described a direct attempt to determine the linear stability of mode-I fracture against bending deformations. Their basic idea was to use a two-dimensional cohesive-zone model of the kind introduced by Dugdale [2] and Barenblatt [3], and to compute the change in the trajectory of a crack induced by an infinitesimally small, static, spatially oscillatory shear stress. In this way, they hoped to learn about the mechanisms that cause roughening of fracture surfaces and that limit the speeds of crack propagation [4,5]. The major part of CLN was devoted to the mathematically difficult job of performing the fully elastodynamic calculation that is needed to determine this perturbed trajectory. CLN concluded that, for cohesive-zone models that do not include dissipative forces, the trajectories are strongly unstable.

Our present investigation has focused, first, on a reexamination of the mathematical problems that emerged in CLN and, second, on an attempt to build into these models some dissipative mechanisms that might provide more realistic descriptions of fracture stability. Our results have been disappointing. The fundamental assumption in CLN was that the Barenblatt-Dugdale cohesive-zone models, suitably generalized to apply to bending non-steady cracks, are robust, mathematically well-posed dynamical systems that incorporate much of the basic physics of fracture in solids. This assumption now seems to be incorrect.

The cohesive-zone models that we have considered have the following properties.

(1) The crack exists on a semi-infinite surface within an isotropic, linearly elastic solid. We shall discuss only two-dimensional cases in which the crack is a line that ends at the crack tip, and the surrounding elastic solid remains in a state of either plane stress or plane strain. The crack-opening displacements, that define the fracture surfaces, are the linear elastic displacements away from the crack line. Note that we exclude consideration of plastic deformation either in the bulk or on the fracture surfaces, and that we also exclude nonlinear elasticity even near the crack tip.

(2) Cohesive forces act between the fracture surfaces and are functions of the crack-opening displacements and their time derivatives. These forces vanish when the crack opening displacements become larger than some fixed range of the interactions; thus there should be a well defined cohesive zone near the tip of the crack within which these forces are nonzero. The cohesive forces may be nonlinear functions of the displacements and may contain dissipative, rate-dependent components; but all nonlinearities and dissipative effects are confined within the cohesive zone.

(3) Real materials cannot support infinite stresses; therefore the elastic stresses must be bounded at every point in the system. As in the original Barenblatt analysis, this finite-stress condition should determine the structure of the cohesive zone uniquely. It should be analogous, for example, to the finite-stress boundary condition at the free end of a moving string.

Implicit in the statement of this third condition is the question of how literally to take the physics of the cohesive zone. Our original idea was that we should not take this aspect of the model literally at all but, instead, should insist that the dimensions of the cohesive zone be the smallest relevant lengths in the theory, and that its dynamic response to external forces plays the role of phenomenological boundary conditions to be imposed at the crack tip. In other words, our cohesive zone should be just a mathematical device for bridging the gap between macroscopic elastodynamics and atomic-

scale mechanisms at the crack tip. There are other possibilities, for example, in polymer fracture where we might develop a model of fibrils forming and breaking within an extended process zone in front of the crack. But, in such circumstances, we would want to add a great deal more detailed physics than we are prepared to consider here.

We have discovered a number of interesting but not entirely reassuring properties of the cohesive-zone models that satisfy conditions (1) through (3) above. Our dissipative models, in all cases where they turn out to be mathematically well posed, exhibit stable crack propagation at small speeds and undergo a transition to instability at larger speeds. We believe that the high-speed instability is associated with the tip-stress anomaly described by CLN. As pointed out in their paper, the tangential stress in all models satisfying the above conditions exceeds the normal (opening) stress everywhere along the crack trajectory, including at the tip, for all nonzero speeds of crack growth. This is a "relativistic" effect; that is, it is a result of the way the stress fields transform to a frame of reference that is moving with the crack tip at some fraction of the sound speed. This extreme form of the conventional Yoffe [6] argument seems, incorrectly as it turns out, to indicate that these models are manifestly unstable for any choice of the cohesive forces — that the forward direction is never preferred by the tip stresses. Our introduction of a dissipative term in the cohesive shear stress does produce stability at small speeds. However, we have serious reservations about this result.

One of our reservations is based on the fact that stabilization at small crack speeds in dissipative models, that turn out to be mathematically well-posed, depend on small-scale features within the cohesive zone, in violation of our intuition that such features should be irrelevant in physically sensible models. A specific, physically implausible aspect of our results is that increasing the strength of the dissipative term in the cohesive shear stress seems always to drive the response of the system in the direction of instability rather than stability.

Our most serious concern, however, is the mathematical fragility that we have found in these models. We have discovered that many, apparently credible choices of cohesive forces lead to mathematically ill posed systems. The equations of motion often fail to have unique, physically acceptable solutions. When acceptable solutions do exist, as mentioned above, they often depend sensitively upon apparently unphysical small-scale features within the cohesive zone. We conclude, therefore, that this particular class of cohesive-zone models — despite its popularity in recent decades — is not suitable for use in theories of dynamic fracture. At the very least, we believe that useful models will have to include plastic deformation in extended regions outside the crack tip, and that they will have to contain enough degrees of freedom to describe the dynamics of blunting at the tip itself.

This report is organized as follows. In Section II we summarize our reformulation of the main results of CLN. We have tried to make this Section readable by relegating almost all mathematical details to a set of Appendices. Those Appendices include analysis which is new and possibly useful for further investigations, but which is peripheral to the main thrust of this paper. Section III is a report on our efforts to include dissipative mechanisms in the steady-state theory, an exercise that seemed to us to be a necessary part of our investigation for reasons that we explain there.

Our principal conclusions emerge in Section IV where we examine the mathematical properties of the equation which determines how an advancing crack responds to bending perturbations. We first point out an unexpected mathematical failure of the CLN analysis. Next, we use a simplified mathematical version of the problem to show how adding a dissipative term to the cohesive shear stress may cure this problem. We then look in detail at stability analyses for the several dissipative fracture models whose steady-state properties are described in Section III. Here we point out that one perfectly plausible model, with apparently all of the necessary ingredients, fails (like CLN) to produce a mathematically well defined response to bending perturbations. We conclude this Section, and the main body of this paper, by describing another model that behaves in much the way we had expected from physical considerations. That is, it is stable at small crack-propagation speeds, becomes unstable at larger speeds, and even, for some values of the dissipation parameters, undergoes a Hopf bifurcation so that the instability occurs at a well defined wavelength. Unfortunately, we have no reason to believe that this model is representative of any broad class of physically motivated fracture models, or that its behavior is a robust feature of such such a class.

II. SUMMARY OF PREVIOUS RESULTS

We start this report by summarizing the strategy and initial results of CLN. In a number of cases, we present those results in forms that are different from the original versions. The reader should refer to CLN and the Appendices in the present paper for a more complete account of the calculations leading to these formulas.

A. Geometry and boundary conditions

The first step in any stability analysis must be the choice of a steady-state configuration whose stability is to be tested. For fracture problems, we need to choose a system that is translationally invariant along the direction of crack propagation. We then must decide upon boundary conditions. There are several ways to pose an elastodynamic boundary value problem so that its solution resembles steady-state fracture.

We might, for example, imagine that a solid containing a crack is truly infinite in extent and is loaded in such a way as to create a concentrated stress at the crack tip strong enough to break the material. If we hold the crack in place by some constraint and then release it, the system must eventually reach steady state in a finite region around the moving tip of the crack. This situation is not well-suited to a stability analysis, however, because the fracture surfaces continue to move away from each other indefinitely far behind the tip, and part of the elastic energy initially stored in the solid is always being carried away to infinity.

A second mathematical device, frequently used in the literature, is to apply moving tractions to the crack faces at some fixed distance behind the tip so that the crack advances steadily at the desired speed. The steady-state solution in this case does not have a wave that propagates to infinity; however this method of controlling the crack extension by adjusting the loading defeats our purpose of studying the stability of a freely advancing crack.

Therefore, like CLN, we consider a crack moving from right to left along the centerline of an infinite elastic strip occupying the region $(-\infty < x < +\infty, -W < y < +W)$ in the x, y plane. Far ahead of the crack, at $x \to -\infty$, the strip is uniformly strained by an amount $\varepsilon_{xx} = \varepsilon_{T\infty}$ (the strain tangential to the crack axis), $\varepsilon_{yy} = \varepsilon_{N\infty}$ (the normal strain) and, for the moment, $\varepsilon_{xy} = 0$. Rigidly clamped boundary conditions at $y = \pm W$ assure that in the steady-state all of the elastic energy initially stored in the strip must be dissipated at the crack tip. From the beginning of the analysis, we assume that the half-width W is very much larger than any other length scale in the problem (the wavelength of the perturbing stress or the length of the cohesive zone), thus we carry out most of our calculations in the limit $W \to \infty$. However, there are several places where we need to reintroduce the length W. For example, the fully relaxed width of the crack must scale like W, and the stress-intensity factor that characterizes the forces transmitted to the crack tip is proportional to $\sqrt{W}$.

To avoid the complication of the fixed grip boundary condition, CLN used a mathematical technique developed by Barber, Donley and Langer [7]. They considered two different boundary-value problems whose solutions are equivalent in a certain limit. The first is the problem described in the last paragraph in which the elastic fields satisfy simple wave equations in the bulk and fixed-grip boundary conditions at a distant boundary. The second is defined in an infinite space, but the fields satisfy a driven massive wave equation with a small mass. If the driving force is proportional to the desired rigid displacement and the mass is proportional to $1/W$, the solutions of the two boundary value problems are equivalent in the limit of very large W.

B. Basic structure of the stability analysis

Suppose that the applied strains $\varepsilon_{N\infty}$ and $\varepsilon_{T\infty}$ are such that the unperturbed crack moves at speed v in the negative x direction along the centerline of the strip. We choose our units of time so that v is measured in units of the transverse sound speed. To examine the stability of this crack, we compute its steady-state response to a small (i.e. first order) external force that produces a spatially oscillating shear stress along the x-axis:

$$\Sigma_{xy}^{(ext)}(x, 0) = \hat{\varepsilon}_m \, e^{imx}. \tag{2.1}$$

The dimensionless stress Σ_{xy} is measured in units of twice the shear modulus, and $\hat{\varepsilon}_m$ is the amplitude of the perturbation whose wavenumber is m. In CLN, $\Sigma_{xy}^{(ext)}$ is defined in the entire x, y plane so that, in principle, it can be the result of tractions applied at the edges of the strip or of material irregularities near the centerline. However, only the value of $\Sigma_{xy}^{(ext)}$ on the centerline is relevant for the first order calculation presented here.

The goal of the calculation is to compute the perturbed centerline $y = Y_{cen}(x)$ of the resulting fracture to first order in $\hat{\varepsilon}_m$, that is:

$$Y_{cen}(x) = \hat{Y}_m \, e^{imx} \equiv \hat{\chi}_Y(m, v) \, \hat{\varepsilon}_m \, e^{imx}. \tag{2.2}$$

(Throughout this paper, symbols with carets such as $\hat{\varepsilon}_m$ and $\hat{Y}_m$ denote Fourier amplitudes.) $\hat{\chi}_Y$ is a complex steady-state response coefficient that depends on the wavenumber m and the average crack propagation speed v. If $\hat{\chi}_Y$ diverges at some v and some real value of m, then we would conclude that the system undergoes a change in dynamic stability at that wavenumber and speed. More generally, poles of $\hat{\chi}_Y$ in the complex m-plane are equivalent to stability eigenvalues. According to (2.2), poles in the lower half m-plane correspond to stable modes, and changes in stability occur when poles cross the real m-axis.

C. Crack-Opening Displacements, Stresses and Cohesive Forces

Let the functions $U_N^{[\pm]}(x)$ be the normal displacements, relative to the local orientation of the centerline $y = Y_{cen}(x)$, of the "upper" $[+]$ and "lower" $[-]$ fracture surfaces. Similarly, let the $U_T^{[\pm]}(x)$ be the corresponding tangential displacements. Then

$$U_N \equiv \frac{1}{2} \left[U_N^{[+]} - U_N^{[-]} \right] \tag{2.3a}$$

is the crack-opening normal (mode I) displacement;

$$U_S \equiv \frac{1}{2} \left[U_T^{[+]} - U_T^{[-]} \right] \tag{2.3b}$$

is the crack-opening shear (mode II) displacement; and

$$U_T \equiv \frac{1}{2}\left[U_T^{[+]} + U_T^{[-]}\right] \tag{2.3c}$$

is the average tangential displacement. (We shall not use U_T explicitly for present purposes, but it is needed in principle for a complete description of the crack surface.)

In a similar way, we define the normal, shear and tangential components of the stress fields evaluated at the fracture surfaces:

$$\Sigma_N(x) \equiv \frac{1}{2}\left[\Sigma_N^{[+]}(x, Y_{cen}) + \Sigma_N^{[-]}(x, Y_{cen})\right]; \tag{2.4a}$$

$$\Sigma_S(x) \equiv \frac{1}{2}\left[\Sigma_S^{[+]}(x, Y_{cen}) + \Sigma_S^{[-]}(x, Y_{cen})\right]; \tag{2.4b}$$

and

$$\Sigma_T(x) \equiv \frac{1}{2}\left[\Sigma_T^{[+]}(x, Y_{cen}) + \Sigma_T^{[-]}(x, Y_{cen})\right]. \tag{2.4c}$$

As before, the subscripts N, S, and T denote tensor components rotated into the local orientation of the centerline Y_{cen}.

The cohesive stress acting between the two fracture surfaces has two components, Σ_{cN} and Σ_{cS}, defined in analogy to (2.4a) and (2.4b) respectively. We assume that these are functions of the local displacements and, when we include dissipative terms, the time derivatives of these displacements:

$$\Sigma_{cN}(x) = \Sigma_{cN}[U_N(x), \dot{U}_N(x)]; \tag{2.5a}$$

$$\Sigma_{cS}(x) = \Sigma_{cS}[U_N(x), \dot{U}_N(x), U_S(x), \dot{U}_S(x)]. \tag{2.5b}$$

In principle, we could include higher time derivatives in these equations. Moreover, in an even more general theory, this local definition of the cohesive forces may need to be replaced by a nonlocal form in which these forces depend on the crack opening displacements everywhere in the plastic zone. We see no compelling physical reason for either of these possible extensions of the present formulation.

In our linear response theory, the shear displacements U_S must be infinitesimally small quantities which vanish when the crack is moving steadily along a straight line. For reasons of symmetry, these quantities can enter the normal cohesive stress only at second order and must therefore be neglected. Similarly, the cohesive shear stress must be linear in U_S and its time derivatives; and it should not depend directly on U_S but, rather, on the shear angle Θ defined by

$$\frac{U_S(x)}{U_N(x)} \equiv \tan\Theta(x) \cong \Theta(x). \tag{2.6}$$

Without loss of generality, therefore, we can write (2.5b) in the form

$$\Sigma_{cS} = \Sigma_{cN}[U_N(x), \dot{U}_N(x)]\left(\Theta(x) + \eta\dot{\Theta}(x)\right), \tag{2.7}$$

where η is a dissipation coefficient and $\dot{\Theta}$ denotes the time derivative of Θ. Our choice of unity for the coefficient of the first factor Θ in (2.7) corresponds to the CLN central-force assumption. That is, apart from the rate-dependent factor $\eta\dot{\Theta}$, the cohesive stress behaves like a central force acting between opposite points on the fracture surfaces.

A general feature of the cohesive stress in these models is that both its normal and shear components must vanish when the crack is fully open, that is, when $U_N(x)$ exceeds the range of the cohesive interactions. We define the cohesive zone to be that region near the tip of the crack, $0 \le x \le \ell$, within which the cohesive forces are nonzero. The length of the cohesive zone, ℓ, is a dynamic quantity that depends on the state of motion of the crack. It appears frequently throughout this analysis.

D. Steps in the CLN Analysis

The CLN analysis starts by transforming the equations of linear elasticity into a frame of reference moving in the negative x-direction at a speed such that the tip of the crack is always at $x' = 0$, that is, $x = x' + x_{tip}(t)$, where

$$\dot{x}_{tip}(t) = -v - \hat{v}_m e^{-imvt}. \tag{2.8}$$

This transformation into a non-uniformly moving frame is essential because it allows us to deal non-perturbatively with the various mathematical singularities that occur at the crack tip. In principle, the new frame should be chosen so that the tip is also at $y' = 0$ in the moving x', y' plane. To first order in the perturbation $\hat{\varepsilon}_m$, however, this extra part of the transformation turns out to be unnecessary. To simplify notation throughout the rest of this analysis, we simply drop the apostrophes after performing the transformation.

The next step in the CLN analysis is to write down formal solutions of the equations of linear elasticity separately in the two regions of the x, y plane above and below $Y_{cen}(x)$, and then to evaluate the unknown coefficients that occur in those solutions by imposing boundary conditions on the centerline. Ahead of the crack tip, the centerline is purely fictitious and the boundary conditions are simply statements that the stresses and displacements must be continuous there. Behind the tip, on the other hand, these boundary conditions are statements about tractions on the fracture surfaces. That is, the stresses at the fracture surface, $\Sigma_N(x)$ and $\Sigma_S(x)$, must be balanced by the cohesive stresses in the cohesive zone and must vanish where the crack is open behind that zone.

It is also necessary, at this stage of the analysis, to separate the problem into parts which are zeroth order and first order in the perturbation $\hat{\varepsilon}_m$. CLN introduced an extra subscript, 0 or 1, to indicate the order at which each function was being computed. That will not be necessary here. All symbols with subscripts N are zeroth order in $\hat{\varepsilon}_m$, and all with subscripts S are first order.

The combination of elasticity and boundary conditions produces a set of Wiener-Hopf equations that can be solved for the unknown stresses ahead of the tip and the unknown crack-opening displacements behind it. At zeroth order in $\hat{\varepsilon}_m$, the equation that relates $U_N(x)$ and $\Sigma_N(x)$ is a restatement of the conventional, steady-state, cohesive-zone model. As in the original analysis of Barenblatt, the condition that the normal stress $\Sigma_N(x)$ remains finite at the crack tip is sufficient to produce a unique solution. At first order in $\hat{\varepsilon}_m$, the equation involving $U_S(x)$ and $\Sigma_S(x)$ contains the information that is needed to find $\hat{\chi}_Y(m, v)$. Again, the condition that $\Sigma_S(0)$ remains finite appears to produce a mathematically well defined equation for U_S. As we shall see, the situation is not so simple.

E. Zeroth Order Problem

The zeroth order, steady-state problem is most conveniently cast in the form of a nonlinear, singular integral equation for the crack-opening displacement $U_N(x)$. (For a more detailed derivation, see Appendix A.) This equation is:

$$\frac{dU_N}{dx} = \frac{1}{\pi b(v)} \int_0^\ell dy \, \sqrt{\frac{x}{y}} \, \frac{1}{x-y} \, \Sigma_{cN}[U_N(y)]; \qquad (2.9)$$

or, equivalently,

$$U_N(x) \equiv \frac{1}{\pi b(v)} \int_0^\ell dy \, Z(x,y) \, \Sigma_{cN}[U_N(y)]$$
$$= \frac{1}{\pi b(v)} \int_0^\ell dy \left[2\sqrt{\frac{x}{y}} - \ln \left| \frac{\sqrt{y}+\sqrt{x}}{\sqrt{y}-\sqrt{x}} \right| \right] \Sigma_{cN}[U_N(y)], \quad (2.10)$$

where the first version of the right-hand side serves as a definition of the kernel $Z(x, y)$. Eqs. (2.9) and (2.10) are valid everywhere in the region $0 \le x \ll W$.

Throughout this paper, all singular integrals such as that appearing in (2.9) denote Cauchy principal values. For simplicity, we have suppressed the argument $\dot{U}_N = v \, dU/dx$ in writing the function Σ_{cN}. The quantity

$$b(v) = \frac{2}{\beta_l v^2} (\beta_l \beta_t - \beta_0^4); \qquad (2.11)$$

plays an important role in much of what follows. Here,

$$\beta_l^2 \equiv 1 - \frac{v^2}{\kappa}; \qquad \beta_t^2 \equiv 1 - v^2; \qquad \beta_0^2 \equiv 1 - \frac{v^2}{2}; \quad (2.12)$$

and the parameter κ is the square of the ratio of the longitudinal to transverse sound speeds. $b(v)$ vanishes at the Rayleigh speed v_R, $b(v_R) = 0$.

The upper limit of integration in (2.9) is the length of the cohesive zone ℓ, defined in the paragraph following Eq. (2.7). Let δ be the maximum range of the cohesive force. Then ℓ is determined by the relation

$$U_N(\ell) = \delta. \qquad (2.13)$$

Equation (2.9) must be supplemented by the Barenblatt condition (non-divergent stress at $x = 0$):

$$\Sigma_{N\infty} = \left[\frac{\kappa}{2\pi \, b(v) \, W} \right]^{1/2} \int_0^\ell \frac{dx}{\sqrt{x}} \, \Sigma_{cN}[U_N(x)] \qquad (2.14)$$

where,

$$\Sigma_{N\infty} \equiv \left(\frac{\kappa}{2} \right) \varepsilon_{N\infty} + \left(\frac{\kappa}{2} - 1 \right) \varepsilon_{T\infty} \qquad (2.15)$$

is the normal stress infinitely far ahead of the crack determined by the applied strains $\varepsilon_{N\infty}$ and $\varepsilon_{T\infty}$.

We also need to know that the energy dissipated per unit length of crack extension is

$$\Gamma_{frac} \equiv \int_0^\ell dx \, \Sigma_{cN}[U_N(x)] \, \frac{dU_N}{dx}. \qquad (2.16)$$

Because the linearly elastic material outside the cohesive zone is energy-conserving, the flux Γ_{frac} defined in this way accounts for the entire conversion of elastic energy to fracture energy in this system. If Σ_{cN} includes dissipative effects, Γ_{frac} will be a function of the crack speed v. If we use first (2.9) and then (2.14) in (2.16), we find

$$\Gamma_{frac}(v) = \frac{1}{\pi b(v)} \int_0^\ell dx \int_0^\ell dy \, \Sigma_{cN}(x) \sqrt{\frac{x}{y}} \, \frac{1}{x-y} \, \Sigma_{cN}(y)$$
$$= \frac{1}{\pi b(v)} \left(\int_0^\ell \frac{dx}{\sqrt{x}} \, \Sigma_{cN}(x) \right)^2 = \frac{W}{\kappa} \, \Sigma_{N\infty}^2. \quad (2.17)$$

The last equality restates the fact that all the elastic energy initially stored in the strip is dissipated at the crack tip. In the limit $v \to 0$, or in the case where the cohesive stress is purely non-dissipative, $\Sigma_{N\infty}$ must be equal to the Griffith threshold stress Σ_G:

$$\Sigma_{N\infty} = \Sigma_G = \left(\frac{\kappa \, \Gamma_0}{W} \right)^{1/2}, \qquad (2.18)$$

where Γ_0 denotes the non-dissipative (threshold) fracture energy.

It will be important to recognize that, outside the cohesive zone where $\ell \ll x \ll W$, (2.10) shows the conventional $\sqrt{x}$ behavior of the crack opening displacement. Only the first term in $Z(x, y)$ contributes in this limit. Thus, with (2.14):

$$U_N(x) \approx \frac{2\sqrt{x}}{\pi \, b(v)} \int_0^\ell \frac{dy}{\sqrt{y}} \, \Sigma_{cN}(y) = \left[\frac{8W}{\pi \kappa b(v)} \right]^{1/2} \Sigma_{N\infty} \sqrt{x}. \qquad (2.19)$$

Note that all of these results so far are completely independent of our specific choice of cohesive stresses.

We shall find it convenient to use a scaled version of the above equations. Indeed, these scaling transformations are needed in order to uncover the mathematical

structure of the problem. Let Σ_0 be some characteristic stress, perhaps the yield stress at the crack tip. Then define

$$\xi = \frac{x}{\ell}, \quad \zeta(\xi) = \frac{\pi b(v)}{\ell\,\Sigma_0}\,U_N(x); \tag{2.20}$$

and

$$\Sigma_{cN}[U_N] \equiv \Sigma_0\,\tilde{\sigma}_{cN}[U_N(x)] \equiv \Sigma_0\,\sigma_{cN}[\zeta(\xi)]. \tag{2.21}$$

Again, we suppress the explicit dependence of σ_{cN} on the derivative of ζ, but must remember in later applications that it may be present. With this notation, (2.9) becomes

$$\frac{d\zeta}{d\xi} = \int_0^1 d\xi' \sqrt{\frac{\xi}{\xi'}}\,\frac{1}{\xi-\xi'}\,\sigma_{cN}[\zeta(\xi')], \tag{2.22}$$

and the Barenblatt condition (2.14) is

$$\Sigma_{N\infty} = \left[\frac{\kappa\ell}{2\pi\,b(v)\,W}\right]^{1/2}\Sigma_0\int_0^1\frac{d\xi}{\sqrt{\xi}}\,\sigma_{cN}[\zeta(\xi)] \tag{2.23}$$

The relation (2.13) that determines ℓ, combined with (2.20), becomes

$$\ell = \delta\frac{\pi b(v)}{\Sigma_0\,\zeta(1)}. \tag{2.24}$$

It is natural, therefore, to measure ℓ and other lengths in the units of δ. We return to this steady-state problem in Section III.

F. First-Order Problem

The CLN result for the response coefficient $\hat{\chi}_Y(m,v)$ has the form

$$-\frac{\hat{\varepsilon}_m}{\hat{Y}_m} = -\hat{\chi}_Y^{-1}(m,v) = im\Delta\epsilon_\infty + \tilde{\mathcal{D}}_0(m,v) + \tilde{\mathcal{D}}_1(m,v) \tag{2.25}$$

where

$$\Delta\epsilon_\infty = \varepsilon_{N\infty} - \varepsilon_{T\infty}. \tag{2.26}$$

It is useful for mathematical purposes — almost essential, in fact — to restrict our attention to the limiting case $m\ell \ll 1$. That is, we look only at perturbations whose wavelengths are very much larger than ℓ, the length of the cohesive zone. As discussed in Section I, we expect ℓ to be smaller than any other relevant length in the system, including $2\pi/m$. Thus this assumption seems reasonable for both mathematical and physical reasons. We shall see, however, that it limits our ability to explore the analytic properties of $\hat{\chi}_Y(m,v)$.

In the small-m limit, the function $\tilde{\mathcal{D}}_0(m,v)$ can be written in the form [see Eq. (B29)]

$$\tilde{\mathcal{D}}_0(m,v) \cong im(-imW)^{1/2}\Sigma_{N\infty}\,\mathcal{D}_0(v). \tag{2.27}$$

The quantity $\mathcal{D}_0(v)$ is a function only of v^2, even for cases in which the cohesive stress contains dissipative terms. $\mathcal{D}_0(v)$ has the limiting value

$$\lim_{v\to 0}\mathcal{D}_0(v) = \left(\frac{\kappa-1}{2\kappa^2}\right)^{1/2}. \tag{2.28}$$

It is a positive, monotonically increasing function in $0 \le v < v_R$, and it diverges as v approaches the Rayleigh speed v_R.

The first two terms on the right-hand side of (2.25) make no reference to the cohesive shear stresses defined in (2.5b) or (2.7). CLN pointed out that these first terms can be obtained by neglecting the cohesive shear stresses but constraining the elastic stress Σ_S to vanish at the crack tip — in effect imposing a "$K_{II} = 0$" constraint. This first part of the response function therefore constitutes a generalization to non-zero velocities of the Cotterell and Rice (CR) [8] quasi-static theory of crack extension. The quantity $-\Delta\epsilon_\infty$ is precisely the CR "T stress"; and the factor $(-imW)^{1/2}$ in (2.27), when included in (2.25), produces a weak (W-dependent) instability for negative values of $\Delta\epsilon_\infty$.

All of the effects of the cohesive shear stress are contained in the third term on the right-hand side of (2.25). In analogy to (2.27), and again in the small-m limit, we can write this quantity in the form [see Eq. (B32)]

$$\tilde{\mathcal{D}}_1(m,v) \cong -m^2\ell(-imW)^{1/2}\Sigma_{N\infty}\mathcal{D}_1(v)\int_0^1\frac{d\xi}{\sqrt{\xi}}\mathcal{S}_{cS}[a(\xi)]. \tag{2.29}$$

Here, $\mathcal{D}_1(v)$, like $\mathcal{D}_0(v)$, is a function only of v^2 and has the same limiting value (2.28) at $v = 0$. It too is a monotonically increasing function of v which diverges, more strongly than $\mathcal{D}_0(v)$, as $v \to v_R$.

The dimensionless quantity $\mathcal{S}_{cS}$ is proportional to the cohesive shear stress given in (2.7). It is defined by

$$\mathcal{S}_{cS}[a(\xi)] = \sigma_{cN}[\zeta(\xi)]\,\tau_{cS}[a(\xi)] \tag{2.30}$$

where

$$\tau_{cS}[a(\xi)] = \left(1 + im\ell\frac{\eta v}{\ell}\right)\,a(\xi) + \frac{\eta v}{\ell}\,\frac{da}{d\xi}. \tag{2.31}$$

Here, we have transformed the linear form $\Theta+\eta\dot{\Theta}$ into the moving frame and have replaced the shear angle Θ by a new function denoted $a(\xi)$. The latter quantity contains much of the interesting structure of the problem. Apart from multiplicative constants [shown in Eq. (B46)], $a(\xi)$ is the ratio of the shear angle Θ to the displacement of the perturbed centerline Y_{cen}; that is, it tells us how much shear is induced by the bending of the crack within the cohesive zone. Note that we have kept a term $im\eta v$ in (2.31); the dissipation length ηv is not necessarily small compared to ℓ, and thus may be comparable to $2\pi/m$.

The equation that determines $a(\xi)$ is deduced from the Wiener-Hopf equation that relates U_S to Σ_S, supplemented by the condition that $\Sigma_S(x)$ be non-divergent at $x = 0$. [See the analysis leading to Eq. (B34).] The result is a linear, inhomogeneous singular integral equation:

$$\frac{3}{2}\sqrt{\xi} = \frac{d}{d\xi}[\zeta(\xi)a(\xi)] - \frac{\beta_t}{\beta_l}\int_0^1 d\xi' \frac{d}{d\xi'}\left[\ln\left|\frac{\sqrt{\xi}+\sqrt{\xi'}}{\sqrt{\xi}-\sqrt{\xi'}}\right| e^{-im\ell(\xi-\xi')}\right] \mathcal{S}_{cS}[a(\xi')]. \quad (2.32)$$

This equation, in the non-dissipative case, is equivalent to Eq. (5.23) in CLN. We discuss it in detail in Section IV of the present paper.

To conclude this summary, we rewrite (2.25) in the form

$$-\hat{\chi}_Y^{-1}(m,v) = im\Delta\epsilon_\infty + im(-imW)^{1/2}\Sigma_{N\infty}\mathcal{D}_0(v)\Phi(m,v), \quad (2.33)$$

where

$$\Phi(m,v) = 1 + im\ell\,\frac{\mathcal{D}_1(v)}{\mathcal{D}_0(v)}\int_0^1 \frac{d\xi}{\sqrt{\xi}}\mathcal{S}_{cS}[a(\xi)]. \quad (2.34)$$

Note that $\hat{\chi}_Y^{-1}(m,v)$ is proportional to im. This is a consequence of translational symmetry in the y-direction; it is the slope of the perturbed trajectory, that is, $im\,\hat{Y}_m$, and not its magnitude that responds to the perturbation $\hat{\varepsilon}_m$. More importantly, the second term on the right-hand side of (2.34), the term that derives from the cohesive shear stress, is explicitly proportional to $im\ell$. We trace this factor to the symmetry requirement that the inclusion of the cohesive shear stress, that is an odd function of the shear angle Θ, can only affect the curvature of Y_{cen} and not its slope.

At first glance, it would seem that we should drop the $m\ell$ term in (2.34) to be consistent with our small-m approximation. In that case, we would have just $\Phi = 1$ and would again recover the Cotterell and Rice theory. The main result of CLN, however, was based on the observation that $a(\xi)$ may diverge at small values of $m\ell$ and v, and that the resulting behavior of $\Phi(m,v)$ in the complex m-plane may completely change the conclusions of CR. For similar reasons, we have retained the factor $e^{-im\ell(\xi-\xi')}$ in the integral kernel in Eq. (2.32), because this factor can play a role at first order in $m\ell$. Other small-m corrections to the kernel are of order $mv\ell$, and thus are doubly small near $m = v = 0$.

Finally, we remark that the ratio $\mathcal{D}_1(v)/\mathcal{D}_0(v)$ in (2.34) is unity at $v = 0$ and diverges as $v \to v_R$. The functions $\mathcal{D}_1(v)$ and $\mathcal{D}_0(v)$ are defined in detail in Eqs.(B30) and (B45). For present purposes, we need to note only that this factor enhances the effect of the cohesive shear stresses at large velocities.

III. STEADY-STATE, UNPERTURBED SOLUTIONS

CLN based their calculations entirely on the standard Dugdale model for which

$$\Sigma_{cN}[U_N(x)] = \begin{cases} \Sigma_0 & \text{for } 0 < U_N(x) < \delta, \\ 0 & \text{for } U_N(x) > \delta. \end{cases} \quad (3.1)$$

Here, Σ_0 is the yield stress that we introduced in (2.21), and δ is the range of the cohesive force defined in (2.13). Although Dugdale interpreted Σ_0 as the plastic flow stress, there is in fact no rate dependent dissipation in this model; all of the stored elastic energy must be converted into the fracture energy $\Gamma_0 = \delta\Sigma_0$. As a result, the crack can advance at any velocity in the range $0 \le v < v_R$ at precisely the Griffith threshold given in (2.18). At higher driving forces, only propagation at the Rayleigh speed v_R can occur with a fraction of the stored elastic energy radiated to infinity.

As pointed out by CLN, the lack of dissipation in the steady-state model is problematic. A linear stability theory is an analysis of the first-order response of a system to some change in the driving force, and such a calculation may not make sense if only one driving force is allowed. The CLN procedure seemed permissible because the only perturbations being considered were shear stresses that bent the crack but did not accelerate it. Once we discovered other difficulties in CLN, however, we realized that we would have to make sure that those problems were not related to this unrealistic aspect of the steady-state behavior. Accordingly, we have examined several dissipative steady-state models, and summarize our results in the next few paragraphs. In short, we find that adding dissipation to the steady state makes some interesting differences in the stability theory but does not make qualitative changes in its mathematical structure.

To start, we need to translate some formulas pertaining to the Dugdale model into the scaled variables introduced in Eqs. (2.20) and (2.21). Because the function $\sigma_{cN}[\zeta(\xi)]$ is unity throughout the cohesive zone $0 < \xi < 1$, we can immediately integrate (2.22) twice to find

$$\zeta(\xi) = 2\sqrt{\xi} - (1-\xi)\ln\left(\frac{1+\sqrt{\xi}}{1-\sqrt{\xi}}\right). \quad (3.2)$$

We then compute the length of the cohesive zone ℓ from (2.24), using $\zeta(1) = 2$:

$$\ell = \frac{\pi b(v)\delta}{2\Sigma_0}, \quad (3.3)$$

which tells us that ℓ is a v-dependent quantity that is of order δ/Σ_0 at small speeds and vanishes at the Rayleigh speed.

The conceptually simplest way of adding dissipation to the Dugdale model was suggested by Glennie [9], who modified (3.1) by writing:

$$\Sigma_{cN}[U_N(x),\dot{U}_N(x)] = \begin{cases} \Sigma_0\,(1+\lambda\dot{U}_N), & 0 < U_N(x) < \delta \\ 0, & U_N(x) > \delta; \end{cases} \tag{3.4a}$$

or, in terms of the scaled variables,

$$\sigma_{cN}[\zeta(\xi)] = \begin{cases} 1+\tilde{\lambda}\,\dfrac{d\zeta}{d\xi}, & 0 < \zeta(\xi) < \tilde{\delta} \\ 0, & \zeta(\xi) > \tilde{\delta}. \end{cases} \tag{3.4b}$$

Here,

$$\tilde{\lambda} = \frac{\lambda v \Sigma_0}{\pi b(v)}; \quad \tilde{\delta} = \frac{\pi b(v)\delta}{\Sigma_0 \ell}. \tag{3.5}$$

Using (3.4b) in (2.22), we obtain an equation that can be solved analytically by standard techniques [10]. The conditions that $\zeta(\xi)$ must vanish at $\xi = 0$ and be positive for $\xi > 0$ are sufficient to determine the solution uniquely. A compact form of the result has been given by Freund [11]:

$$\frac{d\zeta}{d\xi} = \cos\vartheta\,\frac{\xi^{\vartheta/\pi+1/2}}{(1-\xi)^{\vartheta/\pi}}\int_0^1 \frac{ds}{\sqrt{s}}\,\frac{(1-s)^{\vartheta/\pi}}{1-s\xi}, \tag{3.6}$$

where

$$\tan\vartheta = \pi\tilde{\lambda} = \frac{\lambda v\Sigma_0}{b(v)}. \tag{3.7}$$

For the most part, the properties of this solution are what one might expect for a model of this kind. Near the Griffith threshold, (2.18), the crack speed v rises linearly from zero as a function of the stress above the threshold with a slope inversely proportional to the dissipation coefficient λ. For large values of $\tilde{\lambda}$, (that is, for large λv or for v close to v_R where $b(v)$ becomes small), the length of the cohesive zone ℓ goes to a finite value and the energy flux becomes

$$\Gamma_{fract}(v) \approx \frac{\pi^2}{2}\,\Gamma_0\,\tilde{\lambda}(v) = \frac{\pi\lambda\Sigma_0}{2}\,\Gamma_0\,\frac{v}{b(v)}. \tag{3.8}$$

This formula illustrates the behavior of such models in the limit of vanishing dissipation. When λ is very small, v must jump quickly from 0 to values near v_R for a very small increment in Γ_{fract} above the Griffith threshold.

There is, however, one fatal deficiency of this model. For any nonzero value of λv, the stress diverges at $\xi = 1$; and we cannot allow divergent stresses in cohesive-zone models. The divergence is clear in the figures published by Glennie and Freund. To see it from (3.6), note that the integral over s is well defined at $\xi = 1$ for $\gamma > 0$ but the prefactor diverges there. Thus $d\zeta/d\xi$ and, accordingly, $\sigma_{cN}[\zeta(\xi)]$ are unbounded at the back end of the cohesive zone. We therefore must modify this form of the cohesive stress before using it in a stability calculation.

We have examined two qualitatively different forms of the cohesive stress, both of which cure the unphysical singularity at $\xi = 1$. The first was motivated by the idea that the linear, velocity-dependent stress shown in (3.4b) probably ought to saturate at arbitrarily high opening rates. Thus we write

$$\sigma_{cN}[\zeta(\xi)] = \frac{1+\tilde{\lambda}_1\,\dfrac{d\zeta}{d\xi}}{1+\tilde{\lambda}_2\,\dfrac{d\zeta}{d\xi}} \tag{3.9}$$

for $0 < \zeta(\xi) < \tilde{\delta}$. The parameters $\tilde{\lambda}_1$ and $\tilde{\lambda}_2$ are defined in direct analogy with (3.5), with the "bare" parameters now named λ_1 and λ_2. The ratio λ_1/λ_2 determines the highest possible dissipative stress whereas the difference $\lambda_1 - \lambda_2$ is the effective dissipation coefficient for small opening rates.

Another feature of the Dugdale and Glennie cohesive-zone models that may be unphysical is the discontinuity in the stress at the back end of the zone, $\xi = 1$. A simple way to achieve continuity in the cohesive stress without introducing any new parameters is to replace Dugdale's square-law stress function (3.1) by a triangular function that vanishes at $\xi = 1$. That is,

$$\sigma_{cN}[\zeta(\xi)] = \left[1 - \frac{\zeta(\xi)}{\tilde{\delta}}\right]\left(1+\tilde{\lambda}\,\frac{d\zeta}{d\xi}\right) \tag{3.10}$$

for $0 < \zeta(\xi) < \tilde{\delta}$.

Neither of the latter two forms of the cohesive stress produces an analytically solvable version of (2.22), thus we have resorted to numerical methods. In the process, we have discovered that numerical solution of singular integral equations is a difficult and subtle enterprise. Appendix C contains a summary of our strategy and some remarks about the mathematical nature of these problems.

Our numerical analysis indicates that both of the new models, defined by Eqs. (3.9) and (3.10), have non-divergent, physically acceptable solutions. In the saturating case, (3.9), the length of the cohesive zone ℓ vanishes and $\Gamma_{fract}(v)$ reaches a finite limit at v_R. This means that steady-state fracture is possible only for a finite range of driving forces in excess of the Griffith threshold. For the continuous cohesive stress shown in (3.10), on the other hand, the length of the cohesive zone ℓ increases to some limiting value and $\Gamma_{fract}(v)$ diverges like $(v_R - v)^{-1}$ near v_R as in the Glennie model with the discontinuous cohesive stress. We show some representative graphs of $\Gamma_{fract}(v)$ in Figure III.

IV. FIRST-ORDER SOLUTIONS

We turn now to the main effort of this investigation, an analysis of the integral equation (2.32) which should determine the linear response of the crack to bending perturbations. To start, we expand the kernel in (2.32)

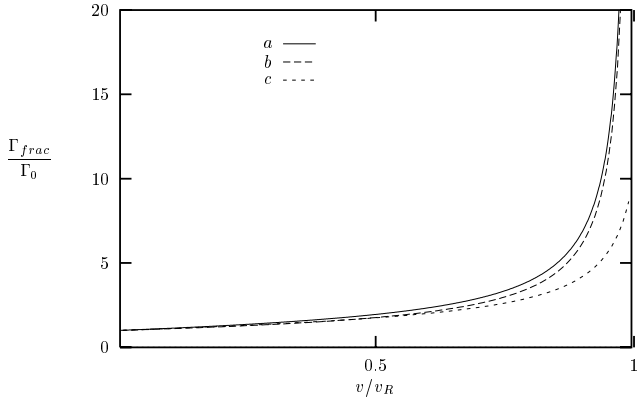

FIG. 1. The theoretical fracture toughness computed for three different normal cohesive stresses. The Glennie cohesive stress (curve a) with $\lambda\Sigma_0 = 1$ produces results similar to the model with the continuous cohesive stress and the same value of λ (curve b). The model with the saturating cohesive stress (curve c) with $\lambda_1\Sigma_0 = 1$ and $\lambda_2\Sigma_0 = 0.1$ leads to a finite fracture toughness at $v = v_R$.

to first order in $m\ell$ and integrate once over ξ. The result is:

$$\zeta(\xi)a(\xi) - \frac{\beta_t}{\beta_l}\int_0^1 d\xi' \Big[Z(\xi,\xi') + im\ell\mathcal{M}(\xi,\xi')\Big]\mathcal{S}_{cS}[\xi'] = \xi^{3/2}, \tag{4.1}$$

where

$$Z(\xi,\xi') = 2\sqrt{\frac{\xi}{\xi'}} - \ln\left|\frac{\sqrt{\xi'}+\sqrt{\xi}}{\sqrt{\xi'}-\sqrt{\xi}}\right|, \tag{4.2}$$

and

$$\mathcal{M}(\xi,\xi') = (\xi-\xi')\,\ln\left|\frac{\sqrt{\xi}+\sqrt{\xi'}}{\sqrt{\xi}-\sqrt{\xi'}}\right| + 2\sqrt{\xi\xi'} - \frac{2\xi}{3}\sqrt{\frac{\xi}{\xi'}}. \tag{4.3}$$

The function $\mathcal{S}_{cS}[a(\xi)]$ is defined in (2.30).

Although they never wrote their equation in this form, CLN were studying the equivalent of (4.1) for the Dugdale model (3.1) and $\eta = 0$, that is, for $\mathcal{S}_{cS}[a(\xi)] = a(\xi)$, when they concluded that this fully dissipationless system was manifestly unstable. They reached this conclusion by noticing that, in the Dugdale case as shown in (3.2),

$$\zeta(\xi) = \int_0^1 Z(\xi,\xi')\,d\xi'. \tag{4.4}$$

Therefore, if one sets $m = v = 0$ in (4.1), so that $\beta_t/\beta_l = 1$, then $a =$ constant is trivially a null right eigenfunction of the operator on the left-hand side (i.e. it is a non-trivial solution of the homogeneous equation). Thus they expected that $a(\xi)$ and, accordingly, the second term in Φ in (2.34), must have a singularity near the origin in the m-plane for small v. By equating coefficients of $\xi^{3/2}$ on both sides of (4.1), they found

$$a \cong \frac{(3/4)}{(1-1/\kappa)v^2 - im\ell} \tag{4.5}$$

which implied a zero in $\Phi(m,v)$ (a pole in $\hat{\chi}_Y$) at $m\ell = i(1-1/\kappa)v^2$. This unstable pole in the upper half m-plane seemed to be consistent with the tip-stress analysis mentioned in Section I of the present paper.

What CLN failed to realize is that the left-hand side of (4.1) is a singular integral operator that has null right eigenfunctions, not just for $m = v = 0$, but for a continuous range of non-zero values of m and v. It is a well known property of singular integral equations such as (4.1) [see [10]] that, like inhomogeneous differential equations, they can have both homogeneous and particular solutions. That is precisely what happens here. The CLN version of (4.1) has no unique solution but, instead, has a continuous, one-parameter family of solutions obtained from a particular solution by adding an arbitrary amount of the null (i.e. homogeneous) solution. We see no physical criterion for selecting among these solutions, thus we conclude that this version of the linear stability theory is mathematically ill-posed.

M. Marder [12] has pointed out to us that the existence of the physically acceptable null eigenfunction of the operator on the left-hand side of Eq. (4.1) means that the steady state solution whose stability we are studying may be non-unique. The null eigenfunction implies, at least in a linear approximation, that the steady state solution can contain symmetry-breaking, shear deformations in the absence of the perturbing shear stress. To compute the amplitudes of these deformations, and to to find out precisely the conditions under which they exist, we would have to carry out a fully nonlinear analysis of the zeroth-order problem including shear crack opening displacements $U_S(x)$ as well as the normal displacements $U_N(x)$. If this interpretation is indeed correct, then what we have identified as a mathematical pathology in the linear response calculation, is an equally pathological lack of definition of the steady-state behavior of these models.

To illustrate the mathematical difficulties, we consider the special case of (4.1) with, as above, $\mathcal{S}_{cS}[a(\xi)] = a(\xi)$ and $m = 0$. This equation has the form

$$\mathcal{L}_\nu * a(\xi) \equiv \zeta(\xi)a(\xi) - (1-\nu)\int_0^1 d\xi' Z(\xi,\xi')a(\xi') = \xi^{3/2}, \tag{4.6}$$

where $\nu = 1 - \beta_t/\beta_l \cong (1-1/\kappa)(v^2/2)$. In Fig. IV, we show null right eigenfunctions of $\mathcal{L}_\nu$, i.e. solutions of $\mathcal{L}_\nu * a_{null}(\xi) = 0$, for various values of ν. These functions $a_{null}(\xi)$ are all perfectly well behaved throughout the interval $0 \le \xi \le 1$; there seems to be no reason to reject them on either mathematical or physical grounds.

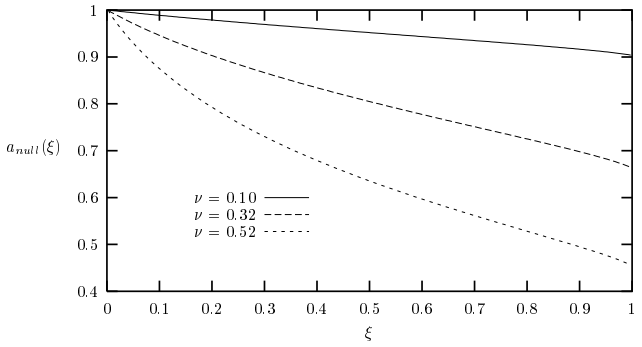

FIG. 2. Well behaved right null eigenfunctions of $\mathcal{L}_\nu$ for three different values of ν.

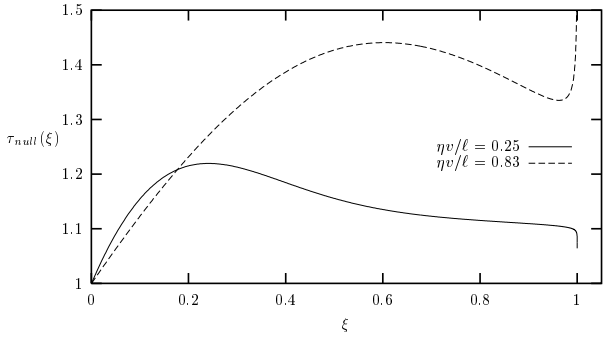

FIG. 3. Right null eigenfunctions of $\mathcal{L}_\eta$ for two values of speed v and fixed $\eta = \delta$ (in our units η is a length and is therefore measured in units of δ as all other lengths are). We have normalized these functions to unity at $\xi = 0$. Note that the coefficient of the singularity at $\xi = 1$ changes sign.

The addition of dissipation changes this situation completely by producing an unphysical singularity in the null eigenvectors and thus a selection mechanism. However, this does not turn out to be the systematic and reliable selection mechanism that we had hoped to find. As a first step in seeing what happens, we look at the same Dugdale steady-state model, again with $m = 0$, but now with a nonzero value of the dissipation constant η. That is, we study

$$\mathcal{L}_\eta * \tau(\xi) \equiv \zeta(\xi)a(\xi) - (1-\nu)\int_0^1 d\xi' Z(\xi,\xi')\tau(\xi') = \xi^{3/2}, \tag{4.7}$$

where

$$\tau(\xi) = a(\xi) + \frac{\eta v}{\ell}\frac{da}{d\xi}. \tag{4.8}$$

For numerical purposes, we find it best to eliminate $a(\xi)$ in favor of $\tau(\xi)$ by writing

$$a(\xi) = \frac{\ell}{\eta v}\int_0^\xi d\xi' \exp\left[\frac{\ell}{\eta v}(\xi'-\xi)\right]\tau(\xi'). \tag{4.9}$$

Note that we have fixed $a(0) = 0$. Our argument for doing so is analogous to one that Langer and Nakanishi [13] used in discussing a model with a similar dissipative term. For nonzero η, we must avoid a discontinuous jump in the shear angle, and therefore a delta-function spike in the shear cohesive stress at the crack tip. For $\eta v \ll \ell$, (4.9) produces a thin boundary layer within which $a(\xi)$ rises rapidly from zero at $\xi = 0$. Here is the first — but unfortunately not the last — occasion in which we shall see a length scale much smaller than ℓ playing a sensitive role in our analysis. As mentioned in Section I, we do not believe that small-scale features of this kind can be taken seriously as physically significant ingredients of our theory; thus we discount results in this regime. Nevertheless, we must find out what happens mathematically.

We have computed the null right eigenfunctions of $\mathcal{L}_\eta$, say $\tau_{null}(\xi)$, and show several of them normalized to unity at $\xi = 0$ in Fig. IV. Most notably, addition of the η term in (4.7) produces power-law singularities at $\xi = 1$ of the form $(1-\xi)^{-\gamma}$. In Fig. IV, we show the exponent γ, determined by fitting the functional form of τ_{null} to a power law in some region around $\xi = 1$, as a function of $\eta v/\ell$ for $\nu = 0.1$. This singularity becomes very weak at small values of $\eta v/\ell$ and therefore makes our numerical analysis difficult in that region. By using smaller and smaller fitting regions, and correspondingly smaller numerical grid spacings, we have estimated γ for values of $\eta v/\ell$ somewhat less than those shown in the Figure. We believe that γ remains positive all the way down to $\eta v/\ell = 0$, implying[1] that all of these null solutions for the stress are divergent and therefore physically unacceptable. The function $\gamma(\eta v/\ell)$ seems not to depend sensitively on ν.

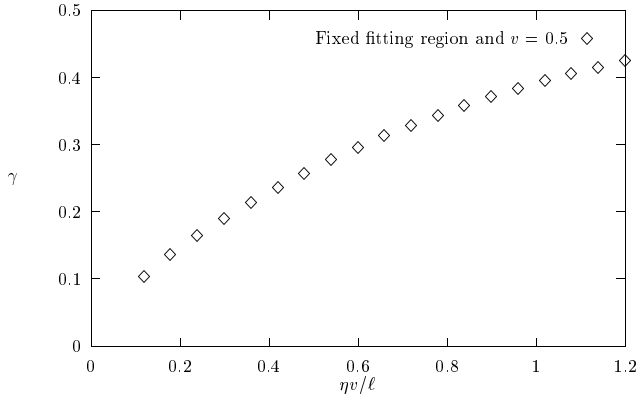

FIG. 4. The exponents of the power law divergence of the solutions at $\xi = 1$ extracted by fitting the functional form of the discrete solution in an interval of fixed width near $\xi = 1$.

We also have computed certain particular solutions of the inhomogeneous equation (4.7), the so-called "minimum-norm" solutions defined in Appendix C. We denote these by the symbol $\tau_{min}(\xi)$, and show several of

them in Fig. IV with parameters corresponding to the null solutions shown in Fig. IV. These particular solutions also have power-law singularities at $\xi = 1$ with the same values of γ as those shown in Fig. IV. The acceptable solutions of (4.7), therefore, have the form

$$\tau(\xi) = \tau_{min}(\xi) + C(v,\eta)\,\tau_{null}(\xi), \tag{4.10}$$

where the factor $C(v,\eta)$ must be chosen so that the singularities in τ_{min} and τ_{null} cancel at $\xi = 1$.

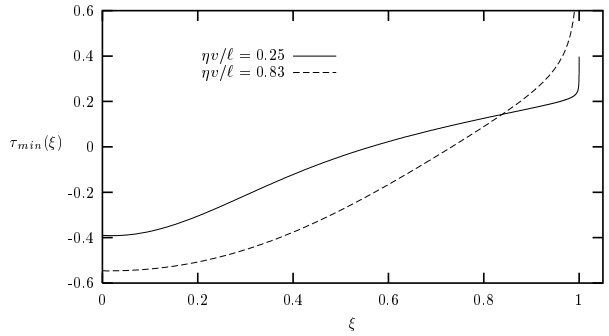

FIG. 5. The minimum norm solutions of the bending response equation with the Dugdale normal cohesive stress. The values of the parameters are identical to those in Fig. IV. Note that the coefficients of the singular part do not change sign.

The resulting solutions for $\tau(\xi)$ or, equivalently, $a(\xi)$ look much like those described by CLN near $v = 0$. The reason for this behavior, as shown in Fig. IV, is that the coefficient of the divergent part of τ_{null}, i.e. $\tau_{sing} \equiv \lim_{\xi\to 1}(1-\xi)^{\gamma}\,\tau_{null}(\xi)$, vanishes at some value of v. Therefore, $C(v,\eta)$ diverges at that value of v, producing a divergence in $a(\xi)$. At and near that value of v, the selected solution $\tau(\xi)$ is dominated by the null solution, which we know is very nearly a constant near $v = 0$. However, the fact that we recover something like the CLN solutions near threshold does not mean that we also recover the CLN instability. As we shall see, the results of the stability analysis are sensitively dependent on the behavior of these weak singularities in the solutions of the integral equation, and crude approximations do not seem to work.

With the understanding that a nonzero dissipation coefficient η may (or may not) determine a unique physically acceptable solution, we return now to (4.1) and report results of numerical solutions with nonzero m and various choices of the normal cohesive stress as described in Section III. In general, once we have found an acceptable set of solutions for $a(\xi)$ for various values of m and v, we can evaluate $\hat{\chi}_Y^{-1}(m,v)$ in (2.33) and look for poles in the complex m-plane. Because mW must be indefinitely large, we can neglect the first term on the right-hand side of (2.33) (the "T stress") and consider only $\Phi(m,v)$ defined in (2.34). Remember that the zeroes of $\Phi(m,v)$ then correspond to the poles of $\hat{\chi}_Y(m,v)$, and that a change in stability occurs whenever a pole

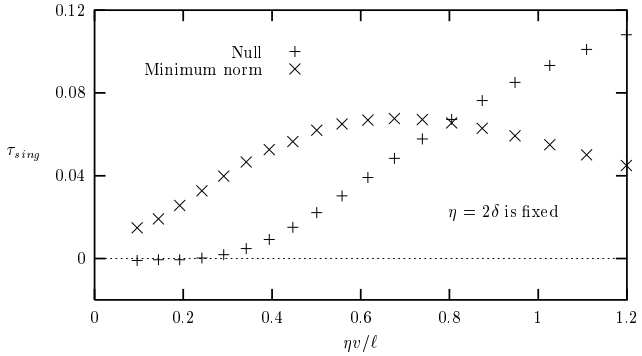

FIG. 6. The coefficients $\tau_{sing} = \lim_{\xi\to 1}(1-\xi)^{\gamma}\tau(\xi)$ of the singular parts of the null and the minimum norm solutions for for a fixed $\eta = 2\delta$.

crosses the real m axis. We emphasize again that, because of the weak singularities in $a(\xi)$ at $\xi = 1$, these calculations become numerically difficult when $\eta v/\ell$ becomes appreciably smaller than unity. This numerically troublesome region is also where we are least confident about the physical basis for our cohesive-zone models.

The simplest non-trivial case is the Dugdale model for the normal cohesive stress, i.e. Eq. (3.1), $\sigma_{cN}[\zeta(\xi)] = 1$, but with nonzero η in the cohesive shear stress factor $\tau_{cS}[a(\xi)]$ defined in (2.31). This is the case in which we thought the stabilizing effect of η should become apparent, and perhaps it does. Indeed, we now find stability at small crack speeds. Recall from our analysis of (4.7) that

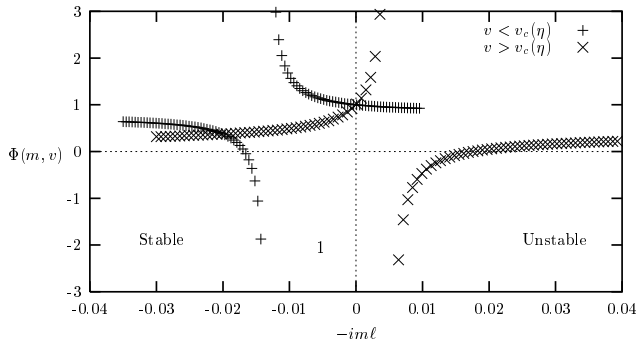

FIG. 7. The dependence of $\Phi(m,v)$ on $-im\ell$ for $\eta = \delta$ and two values of the crack's speed, one above and the other below the critical speed $v_c(\eta)$.

the physically acceptable solution for $a(\xi)$ with $m = 0$ diverges at a non-zero value of the velocity, say $v_c(\eta)$. As a result, the behavior of $\Phi(m,v)$ as a function of $-im\ell$ is radically different for values of the crack speed above and below this critical speed. It is clear from Fig. IV that, for $v > v_c$, the function $\Phi(m,v)$ has a zero in the unstable half of the m-plane, and that the system changes from stable to unstable as v increases through v_c. We plot the position of this zero of $\Phi(m,v)$, i.e. $-im_{pole}\ell$, as a function of crack speed in Fig. IV. The function $v_c(\eta)$ is shown in Fig. IV. Note that v_c decreases with increasing

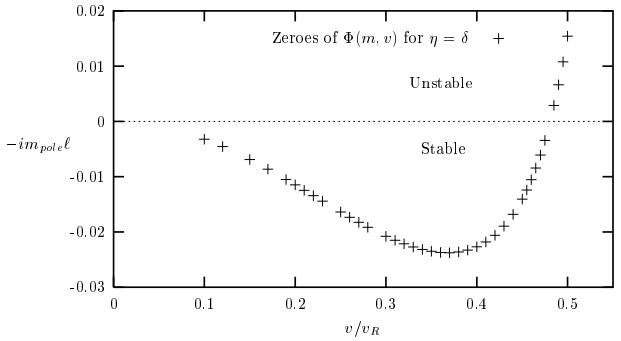

FIG. 8. Zeros of $\Phi(m,v)$ in the complex m-plane plotted as $-im_{pole}\ell$ vs. v/v_R for Dugdale normal cohesive stress. $\eta=\delta$ is fixed. These zeroes are located on the imaginary-m axis.

η, which is perhaps not surprising. The parameter η occurs in our equations only in the combination $\eta v/\ell$, and this term should provide the dominant v-dependence at small speeds. At larger speeds, of course, the "relativistic" v^2 dependence of the other terms in $\Phi(m,v)$ start playing important roles and presumably are responsible for the transition to instability. Because this stability

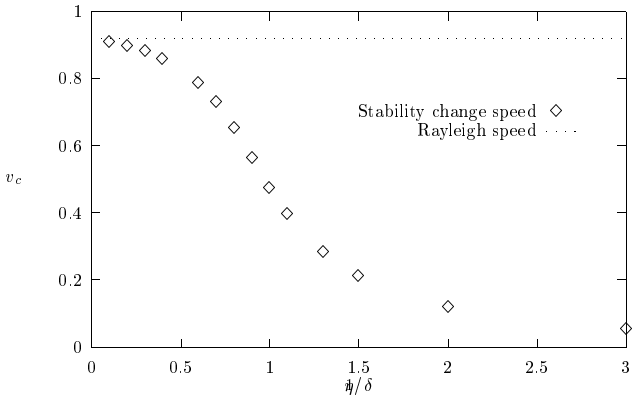

FIG. 9. The critical velocity v_c as a function of the shear dissipation coefficient η for the Dugdale normal cohesive stress.

transition occurs at $m=0$, the interesting behavior takes place at values of $|m\ell|$ that are small enough to be consistent with our approximations. Thus we are forced to the conclusion that increasing the dissipation strength η decreases near-threshold stability in this model. However, the ratio $\eta v/\ell$ is small everywhere in Fig. IV, and actually decreases as η increases. Thus, this apparently unphysical result occurs only in the region where the dissipation length ηv is small compared to the size of the cohesive zone ℓ. If we simply ignore this small-v region and look only at situations where $\eta v \geq \ell$, then we recover something like the CLN instability, i.e. the large-v behavior shown in Fig. IV. But the model then gives us no sensible description of the transition from stability to instability at small velocities. The next case that we examined produced our biggest surprise and our most

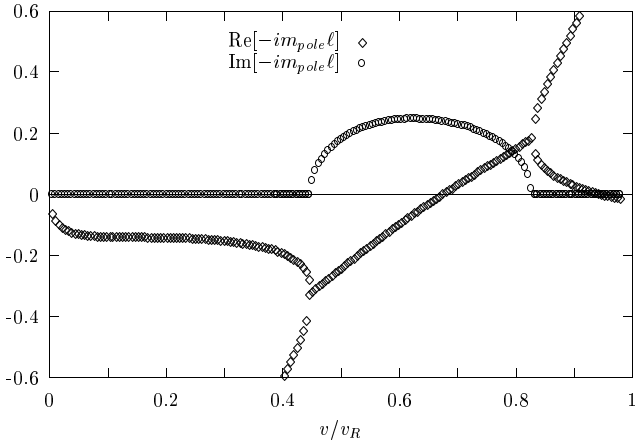

FIG. 10. The real and imaginary parts of the zeros $-im_{pole}\ell$ of $\Phi(m,v)$ in the complex m-plane for the model with rate-saturating dissipation in the normal cohesive stress. The values of the various dissipation coefficients are fixed at $\eta=\delta$, $\lambda_1\Sigma_0=1$ and $\lambda_2\Sigma_0=0.05$.

convincing evidence that this class of models is deficient in important ways. The normal cohesive stress shown in (3.10), for which the non-dissipative factor vanishes continuously at the back edge of the cohesive zone, appears to us to provide a perfectly reasonable model of forces acting at a crack tip. However, when we tried to use (3.10) in the integral equation (4.1), we found a null eigenfunction of of the operator on the left-hand side that, so far as we can tell, has no unphysical singularity anywhere in the interval $0 \leq \xi \leq 1$. [We set $a(0)=0$ as in (4.9) and solved (4.1) for $\tau_{cS}(\xi)$.] We conclude, therefore, that — just as in the much simpler case studied by CLN — this model is mathematically ill-posed for purposes of stability analysis.

We do not claim to understand what it means that an apparently well-posed physical model of dynamic fracture has a mathematically undefined response to infinitesimally small bending perturbations. Nor do we know whether we have accidentally found just one unusually pathological example, or whether many such models behave in this way — perhaps all models with cohesive stresses that decrease continuously to zero at large separations between the crack faces. In any case, this example diminishes our confidence[1] in this approach to fracture dynamics. The one class of models for which we have found somewhat sensible behavior is that for which the normal cohesive forces saturate at high opening rates, i.e. the model shown in (3.9). Just as in the Dugdale model discussed previously, divergences at the back end of the cohesive zone provide a selection criterion, thus the model seems to be mathematically well posed. We have found that adding dissipation to the normal cohesive stress changes some but not all aspects of the behavior of the poles of $\hat{\chi}_Y(m,v)$ while keeping them in the region of the complex m-plane where $|m\ell|$ is small enough to be consistent with our approximations. Some typical results

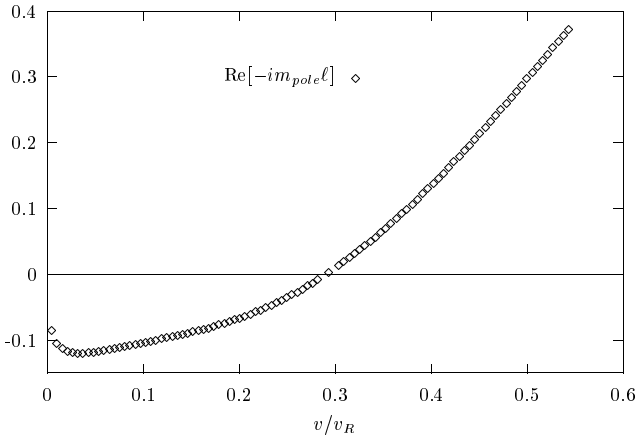

FIG. 12. Same as for Fig. IV except that $\eta = 2\delta$. The imaginary part of the $-im_{pole}\ell$ is not plotted since it vanishes identically for these values of the parameters.

are shown in Figs. IV, IV and IV, where we plot the real and imaginary parts of $-im_{pole}\ell$ as functions of v for two different values of $\eta = \delta$ and $\eta = 2\delta$, and two sets of values of $\lambda_{1,2}$ chosen in such a way as to keep their ratio constant. As before, we find stability at small v and a transition to instability at a critical velocity $v_c(\eta, \lambda_1, \lambda_2)$. The values of $\eta v/\ell$ at the transition are 0.651, 0.510, and 0.513 respectively. Thus we again seem to be in the physically implausible region in which the microscopic length ℓ controls the behavior. For the smaller value of η, the transition is a Hopf bifurcation which determines a characteristic wavenumber, i.e. a nonzero real part of m, at which the initial instability takes place. Increasing dissipation in the normal cohesive stress increases the critical speed thus making the crack more stable. For the larger value of η, the transition occurs at $m = 0$ and, ominously, at a smaller value of v_c. Thus once again we have a situation in which increasing η, i.e. increasing the resistance to shear deformations, reduces rather than increases the threshold for instability.

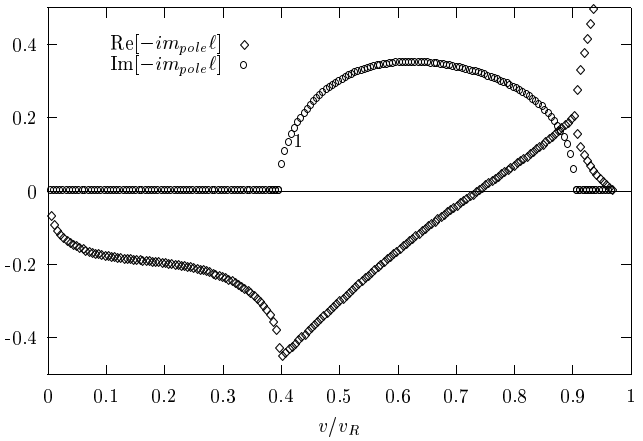

FIG. 13. Same as for Fig. IV except that $\lambda_1\Sigma_0 = 2$ and $\lambda_2\Sigma_0 = 0.1$ so that their ratio is kept constant.

In summary, our results are the following:

The CLN model, which is a simple Dugdale cohesive-zone model with no dissipation in either the normal or shear stresses, is not mathematically well posed for purposes of studying stability of mode-I fracture against out-of-plane bending perturbations.

Similarly, a more complicated and apparently realistic model that contains both normal and shear dissipation, and for which the normal stress vanishes continuously at the back end of the cohesive zone, is mathematically ill-posed. The stability analysis does not make sense for the same mathematical reasons that caused the CLN analysis to fail.

Addition of a simple linear dissipative shear stress converts the Dugdale model into a mathematically well defined system that is stable at the Griffith threshold and undergoes an instability at a higher velocity. However, this behavior depends sensitively on the mathematical structure of the cohesive zone at unphysically small length scales, and therefore seems to depend on artificial features of the model. One symptom of the artificiality of the model is that the critical velocity at which the crack becomes unstable decreases with increasing dissipation strength.

Our fourth, most complex, model, which contains both shear dissipation and a nonlinear dissipative contribution to the normal stress, is mathematically well posed and exhibits physically reasonable behavior at least in some regions of its parameter space. However, like the dissipative Dugdale model, it also loses stability with increasing strength of the shear dissipation. We have no reason to believe that this model is representative of any broad class of physically motivated fracture models, or that its behavior is a robust feature of such a class.

ACKNOWLEDGEMENTS

This research was supported by DOE Grant No. DE-FG03-84ER45108 and also in part by NSF Grant No. PHY94-07194.

[1] E. S. C. Ching, J. S. Langer, and H. Nakanishi, Phys. Rev. E **53**, 2864 (1996).
[2] D. S. Dugdale, J. Mech. Phys. Solids **8**, 100 (1960).
[3] G. I. Barenblatt, Appl. Math. Mech. **23**, 622 (1959).
[4] J. Fineberg, S. P. Gross, M. Marder, and H. L. Swinney, Phys. Rev. B **45**, 5146 (1992).
[5] E. Sharon and J. Fineberg, Phys. Rev. B **54**, 7128 (1996).
[6] E. H. Yoffe, Phil. Mag. **42**, 739 (1951).
[7] M. Barber, J. Donley, and J. S. Langer, Phys. Rev. A **40**, 366 (1989).

[8] B. Cotterell and J. R. Rice, Int. Journ. of Fracture **16**, 155 (1980).
[9] E. B. Glennie, J. Mech. Phys. Solids **19**, 255 (1971).
[10] N. I. Muskhelishvili, in *Singular integral equations*, edited by J. R. M. Radok (P. Noordhoff N.V., Groningen, Holland, 1953).
[11] L. B. Freund, in *Dynamic fracture mechanics*, edited by G. K. Batchelor, G. Wunsch, and J. R. Rice (Cambridge University Press, Cambridge, 1990).
[12] M. Marder, Private communication.
[13] J. S. Langer and H. Nakanishi, Phys. Rev. E **48**, 439 (1993).
[14] W. H. Press *et al.*, in *Numerical recipes in FORTRAN: the art of scientific computing*, 2nd. ed. (Cambridge University Press, Cambridge, New York, 1992), Chap. 2.9, pp. 52–64, and references therein.

APPENDIX A: DERIVATION OF THE STEADY-STATE EQUATIONS

The Wiener-Hopf equations for the steady-state theory are most easily written in a Fourier representation such that, for example,

$$\Sigma_N(x) = \int_{-\infty}^{+\infty} \frac{dk}{2\pi}\, \hat{\Sigma}_N(k)\, e^{ikx}, \tag{A1a}$$

$$\hat{\Sigma}_N(k) = \int_{-\infty}^{+\infty} dx\, \Sigma_N(x)\, e^{-ikx}. \tag{A1b}$$

In this notation, the zeroth order equation [CLN(3.9)] is

$$\begin{aligned}\hat{\Sigma}_N(k) &= \hat{\Sigma}_{cN}^{(+)}(k) + \hat{\Sigma}_N^{(-)}(k) \\ &= 2\pi\Sigma_{N\infty}\delta(k) - \hat{F}(k)\,\hat{U}_N^{(+)}(k)\end{aligned} \tag{A2}$$

The superscripts in parentheses $(\pm)$ indicate functions that have singularities only in the upper (or lower) half k-planes because they are Fourier transforms of functions that are nonzero only on the positive (or negative) x-axis. Thus, the first line of (A2) tells us in Fourier language that the stress $\Sigma_N(x)$ consists of a part $\Sigma_N^{(-)}(x)$ that is nonzero only ahead of the crack, $x < 0$, plus the normal component of the cohesive stress, $\Sigma_{cN}(x)$, which is nonzero for $x > 0$ within the cohesive zone. The second line of (A2) relates these stresses to $U_N(x)$, which is nonzero only behind the crack tip, $x > 0$. The quantities $\Sigma_{N\infty}$ and κ are defined in Section II E.

The Wiener-Hopf kernel $\hat{F}(k)$ is

$$\hat{F}(k) = \left[\left(\frac{\kappa}{2W}\right)^2 + b^2(v)k^2\right]^{1/2} \equiv b(v)\,(\alpha^2 + k^2)^{1/2}. \tag{A3}$$

This expression is a simple interpolation between exact results in the limits $kW \to \infty$ (the only case of direct interest here) and $kW \to 0$. The quantity

$$\alpha \equiv \frac{\kappa}{2\,b(v)\,W} \tag{A4}$$

is infinitesimally small in the limit of very large W. In addition to producing a correct value for $\hat{F}(0)$, its presence here defines the analytic properties of $\hat{F}(k)$ in the complex k- plane.

To solve the Wiener-Hopf equation, (A2), we first factor the kernel (A3):

$$\hat{F}(k) = \hat{F}^{(+)}(k)\,\hat{F}^{(-)}(k), \tag{A5}$$

with

$$\hat{F}^{(+)}(k) = b(v)\,(\alpha + ik)^{1/2}; \quad \hat{F}^{(-)}(k) = (\alpha - ik)^{1/2}. \tag{A6}$$

In terms of these factors, the solutions for the displacement and stress fields are, respectively:

$$ik\,\hat{U}_N^{(+)}(k) = \frac{1}{\hat{F}^{(+)}(k)}\left[\frac{\Sigma_{N\infty}}{\hat{F}^{(-)}(0)} - ik\,\hat{\Lambda}_{cN}^{(+)}(k)\right]; \tag{A7}$$

and

$$ik\,\hat{\Sigma}_N^{(-)}(k) = -\hat{F}^{(-)}(k)\left[\frac{\Sigma_{N\infty}}{\hat{F}^{(-)}(0)} + ik\,\hat{\Lambda}_{cN}^{(-)}(k)\right]; \tag{A8}$$

where

$$\hat{\Lambda}_{cN}^{(\pm)}(k) = \mp \int \frac{dk'}{2\pi i}\,\frac{1}{k' - k \pm i\epsilon}\,\frac{\hat{\Sigma}_{cN}^{(+)}(k')}{\hat{F}^{(-)}(k')}. \tag{A9}$$

A quick way to obtain the condition for nonsingular stress, i.e. the Barenblatt condition, is the following. In (A8), the factor $\hat{F}^{(-)}(k) \sim k^{1/2}$ for large k produces the usual $|x|^{-1/2}$ singularity in the stress at small $|x|$. Both terms inside the square brackets in (A8) are constants at large k; thus the Barenblatt condition is simply the requirement that these constants cancel each other. Specifically,

$$\begin{aligned}\Sigma_{N\infty} &= \hat{F}^{(-)}(0)\int \frac{dk}{2\pi}\,\frac{\hat{\Sigma}_{cN}^{(+)}(k)}{\hat{F}^{(-)}(k)} \\ &= \left[\frac{\kappa}{2\pi\,b(v)\,W}\right]^{1/2}\int_0^{\ell}\frac{dx}{\sqrt{x}}\,\Sigma_{cN}[U_N(x)].\end{aligned} \tag{A10}$$

The second form of this result is the same as that shown in (2.14). We have redundantly inserted the length of the cohesive zone, ℓ, as the upper limit of integration as a reminder that $\Sigma_{cN}[U_N(x)]$ vanishes for larger values of x.

An advantage of this technique is that we can substitute (A10) into (A7) to obtain an expression for $\hat{U}_N^{(+)}(k)$ from which the singularity has been eliminated:

$$ik\,\hat{U}_N^{(+)} = \frac{1}{\hat{F}^{(+)}(k)}\int \frac{dk'}{2\pi}\,\frac{k'}{k' - k + i\epsilon}\,\frac{\hat{\Sigma}_{cN}^{(+)}(k')}{\hat{F}^{(-)}(k')}. \tag{A11}$$

It is now safe and useful to compute the Fourier transform of (A11) and, in doing so, to take the limit $W \to \infty$, i.e. $\alpha \to 0$ in the factors $\hat{F}^{(\pm)}(k)$. The result is Eq. (2.9).

APPENDIX B: DERIVATION OF THE FIRST-ORDER EQUATIONS

Our starting point is the first-order equation [CLN(5.6)] that relates the shear components of the displacement and stress:

$$\hat{\Sigma}_S(k,m) = \hat{\Sigma}_{cS}^{(+)}(k,m) + \hat{\Sigma}_S^{(-)}(k,m) = 2\pi\hat{E}_m\delta(k-m) - \hat{G}(k,m)\,\hat{U}_S^{(+)}(k) + \hat{L}(k,m)\,\hat{U}_N^{(+)}(k-m)\,\hat{Y}_m, \quad \text{(B1)}$$

In analogy with (A2), $\hat{\Sigma}_S^{(-)}(k,m)$ is the Fourier transform of the shear stress in the unbroken region $x<0$, and $\hat{\Sigma}_{cS}^{(+)}(k,m)$ is the Fourier transform of the cohesive shear stress.

The various ingredients of (B1) are:

$$\hat{E}_m \equiv \hat{\varepsilon}_m + im\Delta\epsilon_\infty\hat{Y}_m; \quad \Delta\epsilon_\infty = \varepsilon_{N\infty} - \varepsilon_{T\infty}. \quad \text{(B2)}$$

The function which plays the role of the Wiener-Hopf kernel, the analog of $\hat{F}(k)$ in (A2), is

$$\hat{G}(k,m) = \frac{2}{q_t v^2 (k-m)^2}\Big(k^2 q_l q_t - q_0^4\Big), \quad \text{(B3)}$$

where

$$q_l^2 \equiv k^2 - \frac{v^2}{\kappa}(k-m)^2,$$
$$q_t^2 \equiv k^2 - v^2(k-m)^2,$$
$$q_0^2 \equiv k^2 - \frac{v^2}{2}(k-m)^2. \quad \text{(B4)}$$

Finally, the function which determines the coupling between the oscillating shear stress and the unperturbed crack is:

$$\hat{L}(k,m) = \frac{2\,ikq_l}{v^2}\Big[\Big(\frac{m}{k-m}\Big)^2 - \beta_0^2\Big] \quad \text{(B5)}$$
$$+\frac{2\,ikq_0^2}{q_t v^2}\Big[1 - \Big(\frac{m}{k-m}\Big)^2 - v^2\Big(\frac{k-m}{k}\Big)\Big]$$
$$+\Big(\frac{2\,i}{v^2}\Big)\,|k-m|\Big[\frac{\beta_0^2}{\beta_l}\Big(\beta_l^2 k + m\Big) - \beta_t\Big(\beta_0^2 k + m + \frac{mv^2}{2}\Big)\Big]$$

Despite appearances, $\hat{G}(k,m)$ and $\hat{L}(k,m)$ are finite at $k=m$ and $v=0$.

We now write the Wiener-Hopf kernel (B3) in the form:

$$\hat{G}(k,m) = \hat{G}^{(+)}(k,m)\,\hat{G}^{(-)}(k,m), \quad \text{(B6)}$$

where the superscripts $(\pm)$ have their usual significance. CLN find these factors to be:

$$\hat{G}^{(+)}(k) = \frac{\beta_l\,b(v)}{\beta_t}\,\frac{i(k-k_{R+})}{[\epsilon + i(k-k_{t+})]^{1/2}}\,\exp[N^{(+)}(k)], \quad \text{(B7)}$$

and

$$\hat{G}^{(-)}(k) = \frac{-i(k-k_{R-})}{[\epsilon - i(k-k_{t-})]^{1/2}}\,\exp[N^{(-)}(k)]; \quad \text{(B8)}$$

where

$$N^{(+)}(k) = -\int_{k_{l+}}^{k_{t+}}\frac{dp}{\pi}\,\frac{\varphi(p)}{p-k},$$
$$N^{(-)}(k) = \int_{k_{t-}}^{k_{l-}}\frac{dp}{\pi}\,\frac{\varphi(p)}{p-k}, \quad \text{(B9)}$$
$$\tan\varphi(p) = \frac{p^2|q_l(p)\,q_t(p)|}{q_0^4(p)}; \quad \text{(B10)}$$

and

$$q_l^2(k) = \beta_l^2\,(k-k_{l+})\,(k-k_{l-}); \quad k_{l\pm} = \pm\frac{mv}{\sqrt{\kappa}\pm v} \pm i\epsilon; \quad \text{(B11)}$$

$$q_t^2(k) = \beta_t^2\,(k-k_{t+})\,(k-k_{t-}); \quad k_{t\pm} = \pm\frac{mv}{1\pm v} \pm i\epsilon; \quad \text{(B12)}$$

$$k_{R\pm} = \pm\frac{mv}{v_R \pm v} \pm i\epsilon. \quad \text{(B13)}$$

The quantities k_{t+}, k_{l+}, etc. locate the branch points of $\hat{G}(k,m)$ in the complex k-plane. Note that they are all proportional to mv. The quantities $k_{R\pm}$ are wave numbers for Doppler shifted Rayleigh modes, and are also of order mv.

In the limit $k \gg mv$, the factors $\hat{G}^{(\pm)}$ look very similar to the $\hat{F}^{(\pm)}$ given in (A6):

$$\hat{G}^{(+)}(k,m) \approx \frac{\beta_l\,b(v)}{\beta_t}\,(\epsilon + ik)^{1/2},$$
$$\hat{G}^{(-)}(k,m) \approx (\epsilon - ik)^{1/2}. \quad \text{(B14)}$$

This will be a very useful approximation.

Given the $\hat{G}^{(\pm)}$ (not necessarily in the approximate forms (B14)), we can solve the Wiener-Hopf equation (B1)) for the shear stress and the shear displacement. The results are:

$$i(k-m)\hat{\Sigma}_S^{(-)}(k,m) =$$
$$-\hat{G}^{(-)}(k,m)\Bigg[\frac{\hat{E}_m}{\hat{G}^{(-)}(m,m)} - i(k-m)\,\hat{\Lambda}_m^{(-)}(k,m)\hat{Y}_m + i(k-m)\,\hat{\Lambda}_{cS}^{(-)}(k,m)\Bigg]; \quad \text{(B15)}$$

$$i(k-m)\hat{U}_S^{(+)}(k,m) =$$
$$\frac{1}{\hat{G}^{(+)}(k,m)}\Bigg[\frac{\hat{E}_m}{\hat{G}^{(-)}(m,m)} + i(k-m)\,\hat{\Lambda}_m^{(+)}(k,m)\hat{Y}_m - i(k-m)\,\hat{\Lambda}_{cS}^{(+)}(k,m)\Bigg]. \quad \text{(B16)}$$

Here,

$$\hat{\Lambda}_m^{(\pm)}(k,m) = \mp \int \frac{dk'}{2\pi i}\, \frac{1}{k'-k\pm i\epsilon}\, \left[\frac{\hat{L}(k',m)\,\hat{U}_N^{(+)}(k'-m)}{\hat{G}^{(-)}(k',m)}\right] \tag{B17}$$

and

$$\hat{\Lambda}_{cS}^{(\pm)}(k,m) = \mp \int \frac{dk'}{2\pi i}\, \frac{1}{k'-k\pm i\epsilon}\, \frac{\hat{\Sigma}_{cS}^{(+)}(k',m)}{\hat{G}^{(-)}(k',m)}. \tag{B18}$$

The next step is the analog of the derivation of the Barenblatt condition in (A10). Just as we used the condition that the zeroth-order normal stress be nonsingular at the tip to determine Σ_G in (2.18) and ℓ in, for example, (2.24), so it appears now that we can choose $\hat{Y}_m$ so that the shear stress is nonsingular. As we shall see, however, the situation is not so simple as it seemed in CLN.

On the right-hand side of (B15), in the limit of large k, the factor $\hat{G}^{(-)}(k,m)$ is proportional to $k^{1/2}$ and the quantity in square brackets goes to a constant. Therefore, without regularization, the shear stress would diverge like $|x|^{-1/2}$. Accordingly, we regularize the stress by requiring that the large-k limit of the quantity in square brackets be zero, thus apparently fixing the value of $\hat{Y}_m$. The result is:

$$\begin{aligned}\hat{E}_m &= \hat{\varepsilon}_m + im\Delta\epsilon_\infty \hat{Y}_m \\ &= -\hat{G}^{(-)}(m,m)\int \frac{dk}{2\pi}\,\frac{\hat{L}(k,m)\,\hat{U}_N^{(+)}(k-m)}{\hat{G}^{(-)}(k,m)}\,\hat{Y}_m \\ &\quad +\hat{G}^{(-)}(m,m)\int \frac{dk}{2\pi}\,\frac{\hat{\Sigma}_{cS}^{(+)}(k,m)}{\hat{G}^{(-)}(k,m)}.\end{aligned} \tag{B19}$$

In principle, we can solve (B19) for $\hat{Y}_m$. To do so, we define the function $A(x)$ by

$$U_S(x) = U_N(x)\,\Theta(x) \equiv A(x)\,U_N(x)\,\hat{Y}_m\, e^{imx}. \tag{B20}$$

$A(x)$ needs to be defined only inside the cohesive zone, $0<x<\ell$. It is also useful to define the function $u_S(x)$:

$$U_S(x) \equiv u_S(x)\,\hat{Y}_m\, e^{imx}, \quad \hat{U}_S^{(+)}(k,m) \equiv \hat{u}_S(k-m)\,\hat{Y}_m. \tag{B21}$$

As argued in Section II, the cohesive shear stress is necessarily linear in $u_S(x)$ or, equivalently, in $A(x)$; thus we can write [see (2.7)]

$$\hat{\Sigma}_{cS}^{(+)}(k,m) = \Sigma_0\,\hat{Y}_m \int_0^\ell dx \tilde{\sigma}_{cN}[U_N(x)]\tau_{cS}[A(x)]e^{-i(k-m)x}, \tag{B22}$$

where, in the moving frame of reference,

$$\tau_{cS}[A(x)] = (1+im\eta v)A(x) + \eta v\,\frac{dA}{dx}. \tag{B23}$$

With this notation, (B19) can be rewritten as the formally exact expression for the response coefficient shown in (2.25):

$$-\frac{\hat{\varepsilon}_m}{\hat{Y}_m} = -\hat{\chi}_Y^{-1}(m,v) = im\Delta\epsilon_\infty + \tilde{\mathcal{D}}_0(m,v) + \tilde{\mathcal{D}}_1(m,v) \tag{B24}$$

where

$$\tilde{\mathcal{D}}_0(m,v) = \int \frac{dk}{2\pi}\,\frac{\hat{G}^{(-)}(m,m)}{\hat{G}^{(-)}(k,m)}\,\hat{L}(k,m)\,\hat{U}_N^{(+)}(k-m); \tag{B25}$$

and

$$\begin{aligned}\tilde{\mathcal{D}}_1(m,v) = -\Sigma_0 \int \frac{dk}{2\pi}\,\frac{\hat{G}^{(-)}(m,m)}{\hat{G}^{(-)}(k,m)} \\ \times\int_0^\ell dx\,\tilde{\sigma}_{cS}[U_N(x)]\,\tau_{cS}[A(x)]\,e^{-i(k-m)x}.\end{aligned} \tag{B26}$$

It is useful to write $\tilde{\mathcal{D}}_0(m,v)$ in the form:

$$\tilde{\mathcal{D}}_0(m,v) = \int_0^\infty dx\,h(x)\,U_N(x), \tag{B27}$$

where

$$h(x) = \int \frac{dk}{2\pi}\,\frac{\hat{G}^{(-)}(m,m)}{\hat{G}^{(-)}(k,m)}\,\hat{L}(k,m)\,e^{-i(k-m)x}. \tag{B28}$$

The function $\hat{L}(k,m)$, defined in (B6), is a homogeneous function of k and m of order 2; that is, $\hat{L}(k,m) = m^2\,\hat{L}(k/m,1)$. Similarly, $\hat{G}^{(\pm)}(k,m) = \sqrt{m}\,\hat{G}^{(\pm)}(k/m,1)$. Thus, $h(x)$ is a function only of mx. For $m\ell \ll 1$, $h(x)$ is very slowly varying on the scale ℓ; that is, it changes appreciably only for x of order $1/m \gg \ell$. As a result, the overwhelmingly largest contribution to the integral in (B27) comes from the region outside the cohesive zone and, so long as mW remains large, we can use (2.19) to rewrite (B25) in the form

$$\tilde{\mathcal{D}}_0(m,v) \cong im(-imW)^{1/2}\Sigma_{N\infty}\,\mathcal{D}_0(v). \tag{B29}$$

Here, $\mathcal{D}_0$ is a function only of v [see CLN(6.13)]:

$$\begin{aligned}\mathcal{D}_0(v) = -\frac{1}{(-im)^{3/2}}\left[\frac{2}{\kappa b(v)}\right]^{1/2} \\ \times\int \frac{dk}{2\pi}\,\frac{\hat{G}^{(-)}(m,m)}{\hat{G}^{(-)}(k,m)}\,\frac{\hat{L}(k,m)e^{-ik0}}{[\epsilon+i(k-m)]^{3/2}}.\end{aligned} \tag{B30}$$

(The convergence factor e^{-ik0} is not strictly necessary here.) Its limiting value as $v\to 0$ is given in (2.28). The easiest way to derive (B30) is, in effect, to step backwards and replace $\sqrt{x}$ in (2.19) by

$$\theta(x)\,\sqrt{x} = -\frac{1}{4\sqrt{\pi}}\int dk\,\frac{e^{-ikx}}{(\epsilon-ik)^{3/2}} \tag{B31}$$

where $\theta(x)$ is the unit step function.

There is an important new point here. Despite the appearance of $U_N(x)$ in the formula for $\tilde{\mathcal{D}}_0(m,v)$, the latter quantity is completely independent of what model we use for the cohesive forces so long as we consider only perturbations whose wavelengths $2\pi/m$ are much longer than ℓ.

The formula (B26) for $\tilde{\mathcal{D}}_1$ also can be simplified for the case $m\ell \ll 1$. If we reverse the order of integration in (B26), so that it appears as a real-space integral in analogy to (B27), then the cohesive shear factor limits the integration to the interior of the cohesive zone. As a result, the relevant values of k in the integrand in (B26) are much larger than mv, and we can use the approximation (B14) to write (B26) in the form:

$$\tilde{\mathcal{D}}_1(m,v) \approx -\hat{G}^{(-)}(m,m)\,\Sigma_0 \times \int_0^\ell \frac{dx}{\sqrt{\pi\, x}}\,\tilde{\sigma}_{cS}[U_N(x)]\,\tau_{cS}[A(x)]\,e^{imx}. \quad \text{(B32)}$$

At this point in our analysis, the remaining unknown ingredient of $\hat{\chi}_Y(m,v)$ is the function $A(x)$ appearing in (B32). According to (B20), $A(x)$ describes the bending of the cohesive zone that is induced by the perturbing shear stress. It is the central dynamical variable in this theory.

We must compute $A(x)$ by solving (B16) for the shear-displacement function $U_S(x)$. Equation (B16) is an inhomogeneous linear integral equation that determines $\hat{U}_S^{(+)}(k,m)$, which appears explicitly on the left-hand side and implicitly on the right-hand side *via* the factor $\hat{\Sigma}_{cS}^{(+)}(k,m)$ in $\hat{\Lambda}_{cS}^{(+)}(k,m)$. This equation is best rewritten by using the regularization condition (B19) to eliminate the explicit $\hat{E}_m$, so that the quantity in square brackets on the right-hand side automatically decreases like k^{-1} at large k. The result is [CLN(5.23)]:

$$i(k-m)\,\hat{u}_S^{(+)}(k-m) = \frac{1}{\hat{G}^{(+)}(k,m)}\int\frac{dk'}{2\pi}\frac{k'-m}{k'-k+i\epsilon} \frac{1}{\hat{G}^{(-)}(k',m)}\left[\Sigma_0\int_0^\ell dx\,\tilde{\sigma}_{cS}[U_N(x)]\tau_{cS}[A(x)]e^{-i(k'-m)x} - \hat{L}(k',m)\,\hat{U}_{N0}^{(+)}(k'-m)\right]. \quad \text{(B33)}$$

It is useful — indeed, essential — to invert the Fourier transform in (B33) and study this equation in x- space. We find:

$$H(x) = \frac{d}{dx}\,[A(x)\,U_N(x)] - \Sigma_0\int_0^\ell dy\,\left[\frac{\partial}{\partial y}K(x,y)\right]\tilde{\sigma}_{cS}[U_N(y)]\,\tau_{cS}[A(y)] \quad \text{(B34)}$$

Here,

$$K(x,y) = \int\frac{dk}{2\pi i}\frac{e^{i(k-m)x}}{\hat{G}^{(+)}(k,m)}\int\frac{dk'}{2\pi}\frac{1}{k-k'-i\epsilon}\frac{e^{-i(k'-m)y}}{\hat{G}^{(-)}(k',m)}, \quad \text{(B35)}$$

and

$$H(x) = \int_0^\infty dy\,h(x,y)\,\frac{dU_N}{dy}, \quad \text{(B36)}$$

where

$$h(x,y) = \int\frac{d}{2\pi i}\frac{e^{i(k-m)x}}{\hat{G}^{(+)}(k,m)}\int\frac{dk'}{2\pi}\,\frac{\hat{L}(k',m)}{k-k'-i\epsilon}\frac{e^{-i(k'-m)y}}{\hat{G}^{(-)}(k',m)}. \quad \text{(B37)}$$

In deriving (B34), we have integrated once by parts in the second term on the left-hand side. This is legal because the upper limit of integration, ℓ, is still redundant; $\tilde{\sigma}_{cN}[U_N(x)]$ is defined over the whole positive x-axis and still may be assumed to vanish as smoothly as is necessary for $x > \ell$. There is no difficulty at $x = 0$ so long as the stress remains finite there.

To make further progress we must develop approximate expressions for $H(x)$ and $K(x,y)$ by exploiting the fact that the wavelength of the perturbing stress is much larger than the length of the cohesive zone. We begin by noticing that the expression (B35) for $K(x,y)$ can be obtained from that for $h(x,y)$ in (B37) by replacing $\hat{L}(k',m)$ by 1. Both expressions can be rewritten by defining

$$\Gamma^{(\pm)}(x,m) \equiv \int\frac{dk}{2\pi}\frac{e^{\pm ikx}}{\hat{G}^{(\pm)}(k,m)}. \quad \text{(B38)}$$

Note that $\Gamma^{(\pm)}(x,m) = 0$ for $x < 0$. With the use of these auxiliary functions we can now rewrite (B37) as

$$h(x,y) = e^{-im(x-y)}\int_0^x dx'\,\Gamma^{(+)}(x') \times\int dx''\,L(x'',m)\Gamma^{(-)}(x'+x''+y-x). \quad \text{(B39)}$$

Here $L(x,m)$ is the inverse Fourier transform of $\hat{L}(k,m)$. The expression for $K(x,y)$ can be obtained from (B39) by substituting a delta-function $\delta(x'')$ for $L(x'',m)$

$$K(x,y) = e^{-im(x-y)}\int_0^x dx'\,\Gamma^{(+)}(x')\Gamma^{(-)}(x'+y-x). \quad \text{(B40)}$$

Approximate expressions for $\Gamma^{(\pm)}(x,m)$ can be derived for $mx \ll 1$ by ignoring the small k structure of $\hat{G}^{(\pm)}(k,m)$. Notable exceptions are the contributions to $\Gamma^{(\pm)}$ from the poles at $k = k_{R\pm}$ which become large as v approaches v_R even for small m. We obtain

$$\Gamma^{(-)}(x,m) \cong \frac{1}{\sqrt{\pi x}} - \frac{2i}{\sqrt{\pi}}k_{R-}e^{ik_{R-}x}\int_0^{\sqrt{x}} dt\,e^{ik_{R-}t^2}. \quad \text{(B41)}$$

The analogous expression for $\Gamma^{(+)}(x,m)$ can be obtained multiplying (B41) by $\beta_t/\beta_l b(v)$ and replacing k_{R-} by

$-k_{R+}$. In all the results reported here, we have considered only velocities that are not close to the Rayleigh speed that the second term in (B41) becomes important.

With the assumption that $mv\ell \ll 1$, and the observation that both x and y are small of order ℓ in (B35), we can use the approximations (B14) to find

$$K(x,y) \cong \frac{\beta_t}{\pi b(v)\beta_l}\,\ln\left|\frac{\sqrt{y}+\sqrt{x}}{\sqrt{y}-\sqrt{x}}\right|\,e^{-im(x-y)}. \qquad \text{(B42)}$$

For reasons discussed in Section II F, we have left the factor $e^{-im(x-y)}$ in (B42). Remember that the approximations (B14) are valid for small mv, that is, for small enough v at any value of $m\ell$. The remaining m-dependence in (B42) plays some role near the $v = 0$ threshold.

As in the calculation of $\tilde{\mathcal{D}}_0$ in (2.27), the kernel $h(x,y)$ is a function only of mx and my, and the integral in (B36) is determined accurately, for $m\ell \ll 1$, by values of y outside the cohesive zone. Therefore, in deriving an approximate expression for $h(x,y)$, we may use the small mx approximation only for $\Gamma^{(+)}(x,m)$. Returning to the Fourier transforms, we obtain

$$h(x,y) \cong \frac{\beta_t}{b(v)\,\beta_l}\,e^{-im(x-y)}\int_0^x \frac{dx'}{\sqrt{\pi x'}} \times \int \frac{dk}{2\pi}\,\frac{\hat{L}(k,m)}{\hat{G}^{(-)}(k,m)}\,e^{ik(x-x'-y)}. \qquad \text{(B43)}$$

Since the integral in (B36) is dominated by large values of y, we use (2.19) to find

$$H(x) \cong \frac{3m^2\,(-im)^{1/2}}{2\,\hat{G}^{(-)}(m,m)}\,\frac{\Sigma_{N\infty}\sqrt{W}}{\sqrt{\pi}b(v)}\,\mathcal{D}_1(v)\,\sqrt{x} \qquad \text{(B44)}$$

where

$$\mathcal{D}_1(v) = \frac{4}{3m^2\,(-im)^{1/2}}\left[\frac{2}{\kappa\,b(v)}\right]^{1/2}\frac{\beta_t}{\beta_l} \times \int \frac{dk}{2\pi}\,\frac{\hat{G}^{(-)}(m,m)}{\hat{G}^{(-)}(k,m)}\,\frac{\hat{L}(k,m)\,e^{-ik0}}{[\epsilon+i(k-m)]^{1/2}}. \qquad \text{(B45)}$$

In this case, the convergence factor is necessary. Before reversing the order of integration over k and y, which we have done here, we must close the k-contour in the lower half plane in (B43) because we want $y > x - x'$ in the exponential there. Then, in (B45), the factor e^{-ik0} enforces this closure rule. Unlike the situation in (B30), we would get an incorrect result here if we closed the contour in the upper half plane. We have chosen the prefactors in (B44) and (B45) so that, as in the case of $\mathcal{D}_0(v)$, the function $\mathcal{D}_1(v)$ depends only on v and has the same limit (2.28) as $v \to 0$.

Finally, we make the scaling transformations shown in (2.20) and (2.21), and define $a(x)$ by

$$A(x) = \frac{m^2(-im\pi W\ell)^{1/2}\Sigma_{N\infty}}{\hat{G}^{(-)}(m,m)\,\Sigma_0}\,\mathcal{D}_1(v)\,a(\xi). \qquad \text{(B46)}$$

The result is that (B34) becomes (2.32).

APPENDIX C: NUMERICAL METHODS

The most challenging numerical problems that we have faced in this investigation occur in the inhomogeneous, linear, singular integral equations of the form (2.32) or (4.1), which are to be solved for $a(\xi)$ or, equivalently, $\tau_{cS}[a(\xi)]$. We also have encountered nonlinear singular integral equations in the steady-state problem described in Section III. Here, however, the numerical problems are less severe; there are no weak singularities that need to be resolved in order to select physically admissible solutions.

Our basic strategy has been to replace the unknown function, say $a(\xi)$, by a piecewise-constant approximant that takes on values a_i in intervals $[\xi_{i-1},\xi_i]$, where $\xi_0 = 0$ and $\xi_N = 1$. We have used regular as well as variable interval lengths. Then an integral equation of the form [compare (4.1)]

$$f(\xi)\,a(\xi) + \int_0^1 d\xi'\,Q(\xi,\xi')\,a(\xi') = g(\xi) \qquad \text{(C1)}$$

can be evaluated at points $\xi = z_i \in [\xi_{i-1},\xi_i]$ to become a system of N linear algebraic equations for the N unknowns a_i. We take the $z_i = (\xi_{i-1}+\xi_i)/2$ to be the centers of the intervals. Thus,

$$\sum_{j=1}^{N} C_{ij}\,a_j = B_i, \qquad \text{(C2)}$$

where

$$C_{ij} = f(z_i)\delta_{ij} + \int_{\xi_{j-1}}^{\xi_j} d\xi'\,Q(z_i,\,\xi'), \qquad B_i = g(z_i). \qquad \text{(C3)}$$

In general, C is a non-self-adjoint, complex matrix.

Because the matrix C in all of our applications represents a singular integral operator, it is ill-conditioned in the sense that at least one of its eigenvalues vanishes in the continuum limit, $N \to \infty$. The system of equations (C2) has a homogeneous solution in that limit; that is, (C1) has a solution with $g(\xi) = 0$. In general, particular solutions also exist; therefore we can construct families of solutions by adding arbitrary amounts of homogeneous solutions to particular solutions. Of course, as described in Section IV, not all of these solutions are physically acceptable. In well-posed problems, we expect to be able to exclude all but one of them.

For any large but finite N, C may be a well-conditioned, invertible matrix, but one of its eigenvalues is generally too small for numerical purposes. To deal with this difficulty, we perform a singular-value decomposition [14] of C_{ij} to write it in the form

$$C_{ij} = \sum_k U_{ik}W_kV^{\dagger}_{jk}, \qquad \text{(C4)}$$

where the W_k are the analogs of the eigenvalues of a well-conditioned, i.e. non-singular matrix. (The term "singular", as in "singular matrix" or "singular-value decomposition", refers to non-invertibility of a matrix, i.e. to the existence of null eigenvectors, and not specifically to the singularity of an integral operator in the sense of Muskhelishvili [10].) The matrices U and V are unitary. They are unique up to permutations of columns (and corresponding elements of W) and their columns are left and right eigenvectors of C respectively.

We then use the singular value decomposition (C4) to compute the so-called "minimum-norm" solution:

$$a_i^{min} = \sum_{j,k}{}' V_{ij} \frac{1}{W_j} U_{kj}^{\dagger} B_k, \tag{C5}$$

where the symbol $\sum'$ means that, in the sum over j, we omit the term for which $\lim_{N\to\infty} W_j = 0$. In a finite matrix problem, the vector a^{min} is an exact particular solution of (C2) if the vector B does not lie in the null space of C, and this particular solution would have the smallest possible norm, $\sum_i |a_i|^2$. In our case, although B generally does have a component in the direction of the right null eigenvector of C, the minimum-norm solution (C5) is guaranteed to be well behaved for large N, and it does in fact converge to a particular solution of (C1). We have checked this convergence by computing the residual $\sum_i |\sum_j C_{ij} a_j^{min} - B_i|^2$. This residual was generally of the same order magnitude as the smallest eigenvalue. It vanished in the limit of large N as well.

Using this procedure for the various cases discussed in this paper, we have been able to generate all members of what have always been one-parameter families of solutions. When both the homogeneous solution a_i^{null} and the minimum norm solution a_i^{min} have been found to be singular at $\xi = 1$, the non-singular linear combination has been obtained approximately, up to corrections of order of the mesh interval squared, by the formula

$$a_i = a_i^{null} + \frac{a_N^{null} - a_{N-1}^{null}}{a_N^{min} - a_{N-1}^{min}} a_i^{min}. \tag{C6}$$

We used a regular mesh with $N = 400$ to compute the zeroes of $\Phi(m, v)$ in the complex m-plane that are presented in Figures IV, IV, IV and IV. The detailed study of the $\xi = 1$ singularity in the null and minimum norm solutions of the bending response integral equation 4.1 was done using a mesh with $N = 800$. The spacing of the mesh decreased as a power law near $\xi = 1$ to help achieve greater accuracy in resolving the singularity.